Regulation of Cartilage Metabolism by Dynamic Tissue Shear Strain and the Mechanical Characterization of Cartilage

by

Moonsoo Jin

Submitted to the Department of Mechanical Engineering
in partial fulfillment of the requirements for the degree of

Master of Science

at the

MASSACHUSETTS INSTITUTE OF TECHNOLOGY

February 1999

Author .....
Department of Mechanical Engineering
January, 15, 1999

Certified by .....
Alan. J. Grodzinsky
Professor of Electrical, Mechanical and Bioengineering
Thesis Supervisor

Accepted by .....
Ain A. Sonin
Chairman, Department Committee on Graduate Students

Regulation of Cartilage Metabolism by Dynamic Tissue Shear Strain and the Mechanical Characterization of Cartilage

by

Moonsoo Jin

Submitted to the Department of Mechanical Engineering
on January, 15, 1999, in partial fulfillment of the
requirements for the degree of
Master of Science

Abstract

I investigated the physical regulation of cartilage metabolism induced by dynamic tissue shear strain, and also the mechanical behavior under shear strain, especially focused on shear modulus, under different shear strain, frequency, compressive offset, and physiochemical environment. For this purpose, a new instrument was developed to apply axial deformations as small as 1μm and sinusoidal rotations as small as 0.5% up to 4% based on 1 mm thickness of tissue under feedback control. This apparatus is small enough (30 cm high $\times$ 25 cm $\times$ 20 cm) to be placed in a standard incubator for long-term tissue culture loading studies.

Consistent with previous studies, articular cartilage showed a typical viscoelastic material behavior under shear strain, and the shear modulus increased when the frequency and compressive offset was increased, or the applied shear strain was decreased. This shear softening effect was found to be related to the transient response of cartilage. The equilibrium stress was linear with shear strain. Under different ionic strengths, articular cartilage showed a decrease in the shear modulus up to 1.0 M NaCl bath concentration, but interestingly above this point the shear modulus began to increase while axial stiffness monotonically decreased.

Biosynthetic response of chondrocytes under 0.1 Hz and 1% sinusoidal shear strain, which was measured by the incorporation rate of ^{35}S-sulfate and ^{3}H-proline, was significantly increased compared to the incorporation level of statically compressed or unloaded free-swelling controls. To check the local stimulation by relative fluid flow which can be induced in the outer peripheral region, the incorporation rate of 2 mm center region and outer ring region was compared to those of static and free swelling controls. Unlike axial compression, where the incorporation rate in the outer ring region was greater than the 2 mm center region due to fluid flow and cell

deformation, the effect of shear strain was uniformly distributed over the entire area, so the increased biosynthetic effect under shear strain is more related with direct mechanical deformation of chondrocytes rather than fluid flow, changes in hydrostatic pressure, or electrical or chemical environment.

Thesis Supervisor: Alan. J. Grodzinsky
Title: Professor of Electrical, Mechanical and Bioengineering

Acknowledgments

I came to the USA on July 10, 1997 for the first time in my life. Al was the the first, last, and the only professor whom I met to offer me an RA position. My work experience with the shear force on endothelial cells began when I was in Korea seemed appealing to him at our first interview. Al was always welcoming and encouraging to students, and sometimes I felt more motivated due to his always friendly attitude.

Most of my work was done together with Marc Levenston, who left here to be a professor at GIT. He showed me how I should behave in order to become a real scientist. Then there's Eliot, who helped out from the design of the mechanical components for our machine to all other kinds of computer work. Fred Cote, who is a technical instructor at Edgerton student machine shop, helped me machining every components for the apparatus. Thanks, Fred.

Also I'm greatly indebted to Hanhwa and Linda. Without their help this lab could not operate normally. Then Emo, whom I took Thermo with. It was a fun to discuss entropy and enthalpy transfer.

I also shouldn't forget my office mate, Bodo, a postdoctoral fellow from Germany. Through his life, I've learned what life should be. Special thanks to Parth who will be a good friend during our PhD course. Also I'd like to thank the other present and past members - Steve, Paula, Andy, Jeff, JT, Cyndi, Vicki, Bryant, and Niti.

Finally, last but not least, I married Miwan on September 6, 1998. She is the love of my life whose strength has always encouraged me to do my best. My sincere thanks to Professor Min who has given me directions in many ways. In closure I would like to thank my family for their love and guidance.

Contents

List of Figures

List of Tables

Chapter 1

General Introduction

1.1 Cartilage Structure and Function

Articular cartilage is the opaque covering of the ends of synovial joints and its major function is load bearing and reducing friction between joints. Chondrocytes produce and maintain the extracellular matrix of cartilage, a tissue that is resilient and pliant [33].

Articular cartilage consists of about 80% of water by wet weight, cells less than 10% by volume, and the extracellular matrix [42, 30, 34]. The extracellular matrix is composed principally of hydrated collagen fibrils (50-60% of tissue dry weight), large proteoglycans (30-35% dry weight) and noncollagenous proteins and glycoproteins (10-20% dry weight) [30, 34, 15] (Figure 1-1). The biomechanical and electromechanical properties of cartilage come from the combined effect of the collagen fibrils and proteoglycans. The collagen fibrils, which are predominantly type II in articular cartilage, provide strength in tension and shear, and the electrical repulsion and osmotic swelling due to fixed-charge in proteoglycans withstand the compressive load [29]. Due to the interaction between collagen and aggregated proteoglycan, cartilage is constantly under the balance between swelling pressure and tension, and this property endows cartilage with its load-bearing ability.

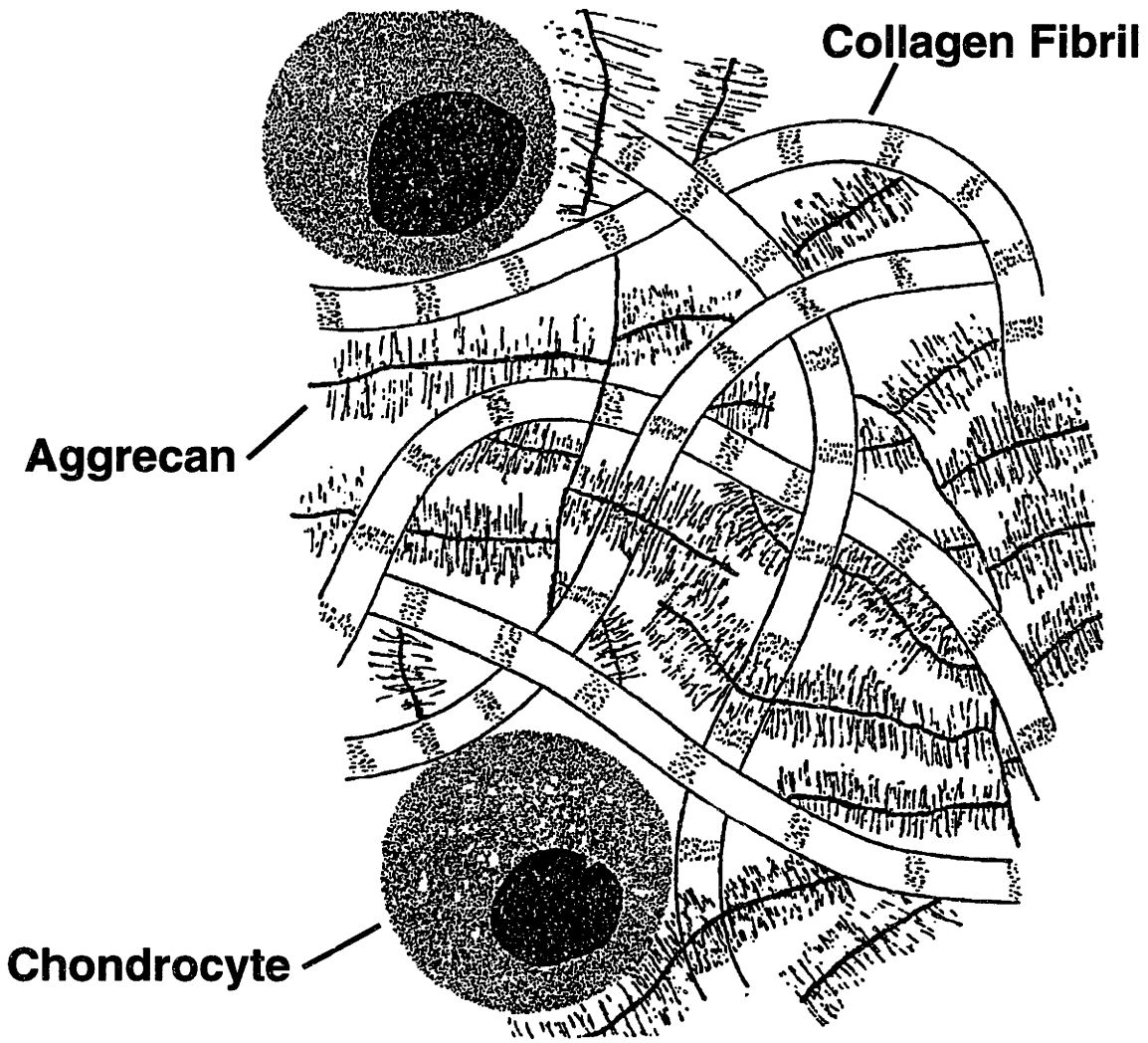

Figure 1-1: Schematic drawing of articular cartilage structure. Extracellular matrix is mainly composed of collagen fibrils and aggregated proteoglycans.

Collagens are composed of three polypeptide chains (α-chains), each possessing a characteristic tripeptide sequence (gly-x-y) that forms a left handed helix. Frequently, X is proline and Y is hydroxyproline. Among the many different collagens, fibrillar type II collagen is specific to cartilage and is a marker of chondrocytes differentiation [33]. Type II collagen forms cross links with type IX collagen, and the antiparallel orientation allows cross linking between different fibrils and permits limited deformation under mechanical compression [9].

The load bearing function of cartilage depends essentially on the properties of the large cartilage-specific proteoglycan which is immobilized in the collagen network. It is a bottle brush structure with a core protein to which are attached laterally along its length as many as 100 chondroitin sulphate chains and 30 keratan sulphate chains, and many proteoglycan molecules can bind to a single chain of hyaluronan with high affinity to form huge multimolecular aggregates [36]. The binding of proteoglycan molecules to hyaluronan is further stabilized by the interaction with link protein, which is relatively small glycoprotein. Aggrecan and link protein bind to each other via immunoglobulin folds to form tertiary complexes with hyaluronan [7], and these aggregates are large enough to be immobilized within the collagen network.

1.2 Mechanical Behavior of Cartilage under Shear Strain

The deformational behavior of articular cartilage is regulated by 1) the interstitial fluid flow through the porous matrix, which is opposed by the frictional drag between the fluid and matrix components, or 2) the intrinsic characteristics of extracellular matrix, collagen and aggrecan. Typically this deformational behavior follows the viscoelastic material characteristics, which combine the solidlike and liquidlike characteristics, and researchers have modeled this behavior using poroelastic theory [11, 14, 27] or biphasic mixture theory [31, 26] when the deformation induces relative fluid motion within the matrix, or one phase viscoelastic theory using Fung's quasi-

linear viscoelastic theory [21, 52, 44, 46, 55]. In this thesis, the mechanical behavior of articular cartilage was measured under pure shear or simple shear strain conditions. Dynamic shear modulus was calculated based on the recorded displacement and torque data under different mechanical conditions, and the relation between dynamic shear modulus and the change in shear strain, frequencies, and compressive offset was described. To see the effect of physicochemical and electrical environment on the extracellular matrix, the axial and shear modulus were measured under different ionic strengths.

1.3 Effects of Matrix Shear Strain on Cartilage Metabolism

Physical regulation plays a significant role in the development and maintenance of normal articular cartilage. Various loading-induced physical phenomena (fluid pressure, cell/matrix deformation, streaming potential, etc.) have been proposed to play different roles in metabolic regulation [16, 18]. Several *in vitro* studies of physical regulation of cartilage metabolism have utilized various mechanical stimuli such as dynamic compression [41, 6], cyclic hydrostatic pressure [19], and fluid induced shear stress [45]. Dynamic compression is particularly complex, inducing volumetric changes, shear stresses, and gradients in intratissue pressure and fluid flow, which have been spatially associated with metabolic stimulation [24].

To decouple the mechanical regulation from the other effects of chemical or electrical environment change, or interstitial fluid motion, we designed a machine which can apply shear strain on tissue, since macroscopic shear deformation of a poroelastic tissue such as articular cartilage should not induce volumetric changes, intratissue fluid flow or pressure gradients. While investigators have examined fluid-induced shear stress in monolayer cell culture [45, 53], we know of no studies of the effects of macroscopic shear deformation of tissue explants on chondrocyte metabolism.

1.4 Thesis Overview

In this thesis, the objectives were 1) to design a machine which can apply shear strain on cartilage for mechanical and biological experiments; 2) to characterize the mechanical behavior of articular cartilage under different mechanical conditions, such as strains and frequencies of sinusoid, compressive offset, and different bath ionic concentration; and 3) to investigate the effect of matrix shear strain on the biosynthetic response of chondrocytes.

In chapter II, the newly designed shear application instrument is described, focusing on the design of the shear loading apparatus and its performances. Each component is shown separately, and a complete schematic drawing is included in the Appendix. Chapter III shows the change in shear modulus under different mechanical and physicochemical conditions. The results of the effect of macroscopic shear on cartilage metabolism were shown in Chapter IV. General conclusion and future work were made in Chapter V.

Chapter 2

Machine Design

2.1 Machine Configuration

We have developed an incubator housed, biaxial loading device capable of applying axial sinusoidal movement as small as 1 μm and sinusoidal rotations as low as 0.01 degree (Figure 2-1. For detailed drawing, refer to Appendix). The philosophy of the design was to make the machine to be rigid, versatile, and each components to be easy to control and upgraded. The machine is supported by three 25.4 cm diameter stainless steel rods and top and bottom plates. A third stainless steel plate was clamped to the support rods to allow repositioning for different experimental shear and compression chambers. A linear motion is activated by a stepper motor and guided through two linear bearings and three supporting rods. Two limit sensors keep the linear motion within the control range. The rotational movement is made by a rotary positioning table which is activated through a 180 to 1 worm gear combination. By using this table the rotational motion gives high torque and resolution, and low backlash. This machine has several sensors, two LVDT which feed the linear and rotational position data to the controller, load cell and torque transducer which measure normal and shear forces applied to tissue. By attaching two sheet springs to linear motion guide, the backlash of linear motor is reduced to nearly zero. By feeding the LVDT, and load and torque cell data, the biaxial motion can be controlled based on the position or force which can be used for creep test. The overall size of this

machine is small enough (30 cm high × 25 cm × 20 cm) to be housed in an incubator for long-term tissue culture loading studies.

2.1.1 Motors

Motor for Axial Movement: Linear Stepper Motor (23A-6102A, American Precision, Buffalo, NY)

Motor for Rotational Movement: Linear Stepper Motor (23D-6303, American Precision)

A linear stepper motor for the axial movement has a threaded rotor which engages a threaded rod. The threaded rod in turn is attached to a carriage plate and pair of linear bearings which ride on two of the support rods. The axial motor is capable of applying compressive ramps at rates up to 1 mm/sec with an applied force up to 400 N. The movement of rotational motor is connected to a rotary position table through a worm gear combination. Each motor is driven by a micro-stepper drive (IM483, Intelligent Motion Systems, Marlborough, CT). The drives are electrically isolated via internal opto-couplers and each have their own power supply separate from the analog and digital electronics power supply. The micro-stepper drives combined with the motors and gearing provide a theoretical axial resolution of 50 nm and rotational resolution of 0.0005 degree.

2.1.2 Rotary Positioning Table

Model: 6R180, Design Components, Franklin, MA

This table features a rigid pair of angular contact bearing and 180 to 1 worm gear drive.

2.1.3 Sensors

LVDT: Axial and angular displacement measurement: Linear variable differential transformers, (LVDT, Model S5, Sensotec, Columbus, OH).

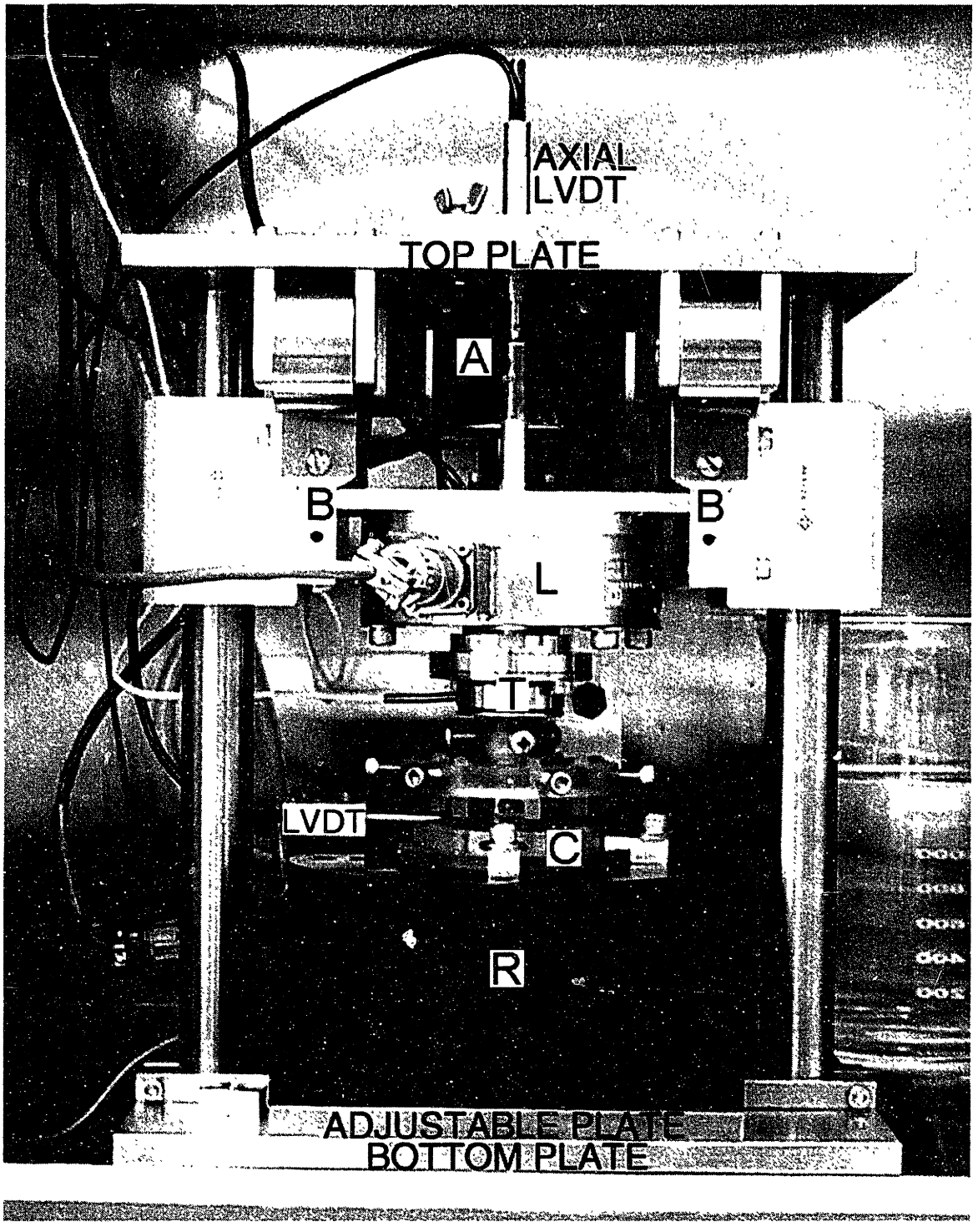

Figure 2-1: Shear/compression apparatus: A—Axial linear stepper motor; B—Bearing/carriage assembly; C—Sample chamber; L—Load cell; T—Torque cell; R—Rotary position table. The adjustable plate may be moved to accommodate other fixtures. The LVDT shown to left of chamber (C) senses rotational displacement. Rotary table (R) is driven by stepper motor behind the table.

A block is placed at 6.35 cm from the center of the rotating table, and LVDT contacts it to measure angular displacement. For small angular rotations, the displacement of the block sensed by the LVDT is essentially a linear function of angular rotation.
Load cell: Model: 10N, 100N, and 500N capacities (Model 31, Sensotec)
Torque cell: Model: 5N-m capacity (Transducer Techniques, Temecula, CA), 0.2N-m capacity (QWLC-8M, Sensotec)
Various load transducers and torque transducers can be rigidly attached in series between the carriage and sample chamber to measure compressive and shear stress in the samples. Rotational control is integrated with axial control so that shear tests can be intermixed with compression tests in the same experimental procedure.

2.1.4 Chambers

Dynamic Shear Chamber: Chambers were designed considering for the application of shear strain and also axial strain, and twelve samples can be located circumferentially at each well. The recent chamber (Figure 2-2) was modified for its compressing rods can be adjusted for the even contact between samples and rods.
Control Chamber: Conventional chamber is used for static and free swelling control [41] (Figure 4-3).

2.1.5 Control and Data Acquisition

The control electronics, including the transducer signal conditioners for the LVDT's, load cells, and torque cells as well as the limit, feedback, and digital switching circuits were mounted on two prototype circuit boards with copper cladding acting as a ground plane. A digitally-controlled analog switch allows any one of the axial displacement, angular displacement, axial load, or torque signals to be used for closed-loop feedback control. A computer-based data acquisition system provides control and monitoring of the apparatus. The data acquisition and control subsystem consists of an multi-function I/O card (AT-MIO-16DL-9, National Instruments, Austin, TX), which provides high-speed analog-to-digital conversion (ADC) and digital I/O,

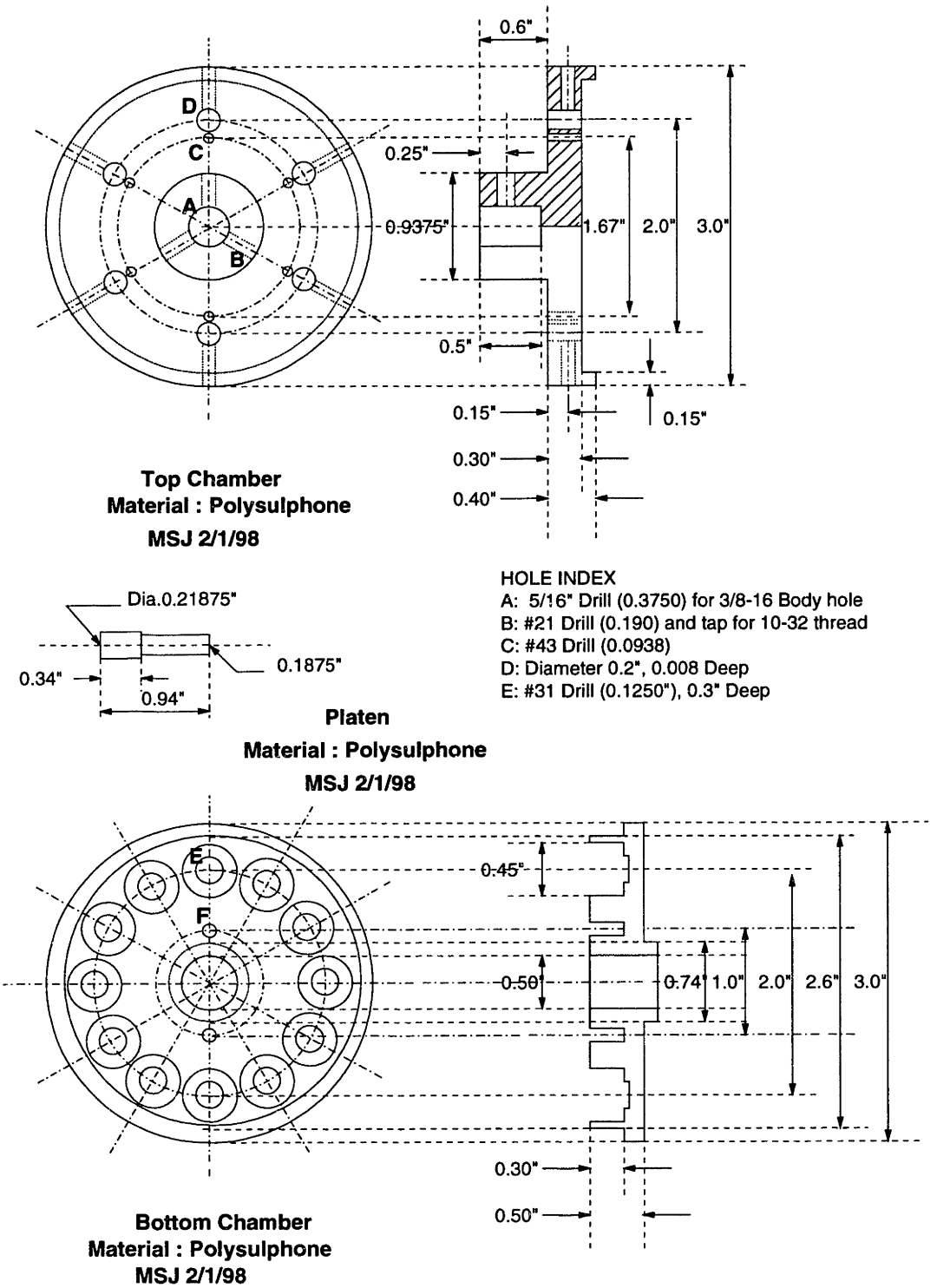

Figure 2-2: Top chamber, bottom chamber, and platens. The platens are assembled into the holes in top chamber, and after loading cartilage specimens, platens are falling on top of specimens by their weight when bolts are loosened, and platens are fixed after that.

and a 10-channel digital-to-analog converter (DAC) board (AT-AO-10, National Instruments). The DAC channels provide signal offsets as well as ramp and sinewave control signals. In axial displacement feedback control, sinusoid waveform distortion is less than 1% for a 10 μm amplitude sinewave, comparable to that of our Dynastat mechanical spectrometer (Dynastatics, Albany, NY) ($\sim$ 0.3%) which we have used in our previous studies on cartilage metabolic response to dynamic compression [41].

2.2 Performance

This machine can be operated under two distinct modes. In the pure shear mode (PSM) a cartilage disk is located aligned with the axis of rotation, and it is deformed under pure torsional shear. Under simple shear mode (SSM), multiple cartilage samples are located in the dynamic shear chamber wells at a given radius from the center axis of the chamber, and they can be assumed to be under simple shear application (Figure 2-3). To check whether slipping between specimens and platens of chamber occurs, shear modulus was measured using sand paper attached to bottom chamber and platens to prevent slipping, and the results were compared with normal condition (no sand paper) under PSM. By analyzing the torque wave form and harmonic distortion, the slipping seems to occur above 3% of shear strain under SSM. To compare the shear modulus under PSM and SSM, disk specimens 8.4 mm diameter by 1mm thick were prepared, and the dynamic shear modulus was measured under PSM. Four 3 mm diameter samples were separated out of it, and under SSM dynamic shear modulus was measured, and the shear modulus under two different modes was compared. Difference of the magnitude of shear moduli between two different modes was less than 10% of the magnitude (data not shown).

Even though the machine itself is much more stiffer than specimens, torsional and axial compliances of the machine were measured and taken into account for the calculation of the axial stiffness and shear modulus of the specimens.

2.2.1 Shear Application Mechanism

Cartilage plugs can be placed aligned with the center of the table (PSM, pure shear mode), and for cell culture experiments cartilage specimens were placed circumferentially in the dynamic shear chamber (SSM, simple shear mode)(Figure 2-3). Under simple shear mode (SSM), shear strain on sample is maximal at distal edge and minimal at proximal edge from the center, which is 1.06%, 0.94% respectively, when 1% shear strain is applied on the center line of sample. So it can be assumed that samples are under simple shear strain.

2.2.2 Axial and Rotational Compliance

Even though the machine itself is much stiffer than samples, all sensors and chambers are assembled and under higher frequency and large displacement measurement, the axial and torsional compliance of specimens can reach 10% of the modulus of shear loading apparatus. Axial and torsional compliance of the machine were measured under 10 N compressive offset under different frequencies and strains. The measured compliances were essentially insensitive to frequencies and applied strain. The axial and rotational (Figure 2-4) compliances (1.114 μm/N and 1.05 mdeg /Nm, respectively) were taken into account for the calculation of axial stiffness and shear modulus of samples.

2.2.3 Shear Modulus Calculation

Dynamic shear modulus is calculated separately for pure shear and simple shear mode:

Pure Shear Mode

Engineering shear strain in the sample located at the center of rotation is computed as the rotational angle (θ) times the specimen radius (R) divided by sample thickness (h):

$$\gamma = \theta \times R/h \, . \tag{2.1}$$

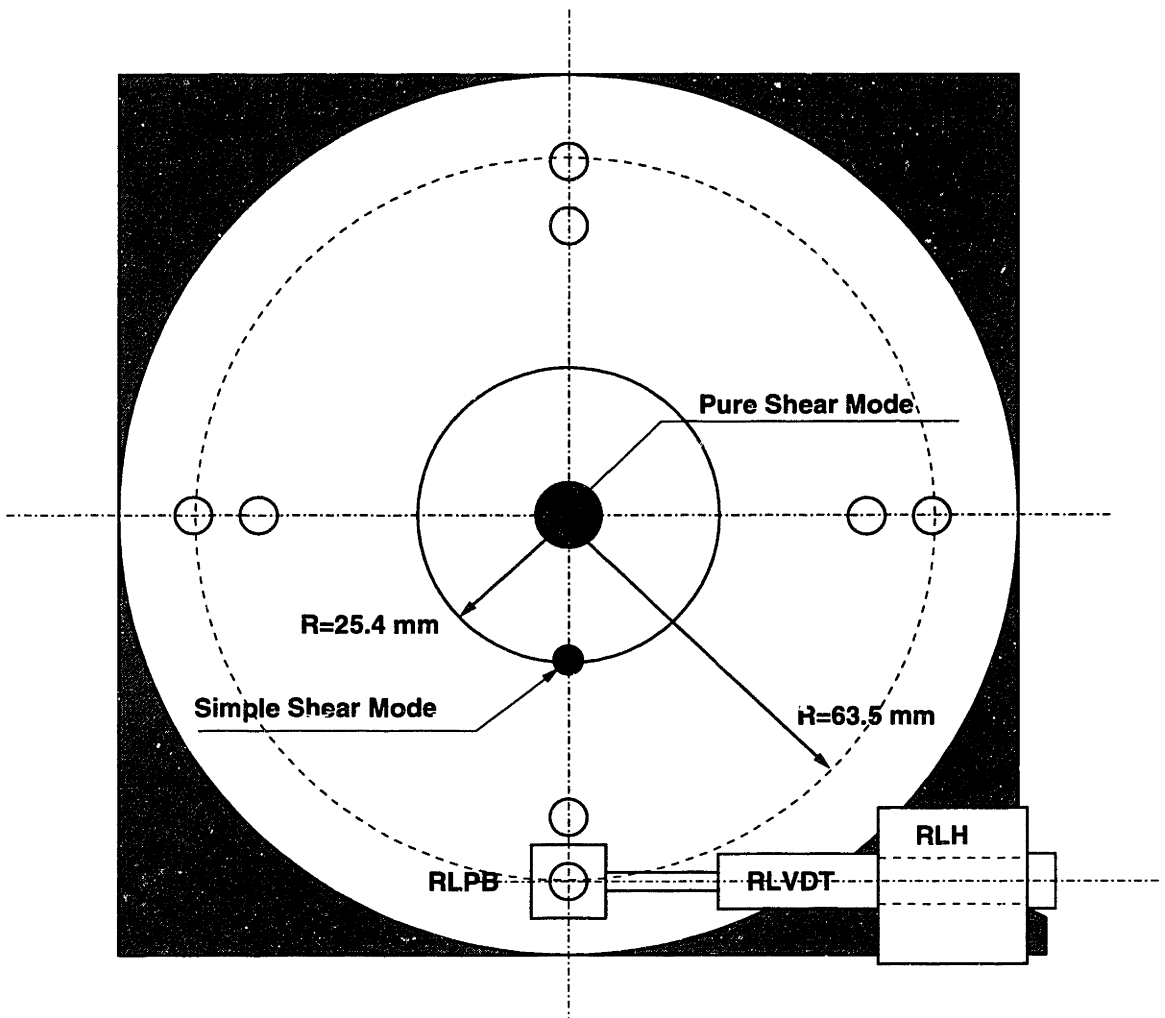

Figure 2-3: Top view of Rotary Positioning Table (RPT). Samples are displayed in two different modes ,PSM and SSM. LVDT (RLVDT) measures the angular movement, and for less than 0.1 degree, displacement at LVDT can be converted to the rotational angle with negligible error.

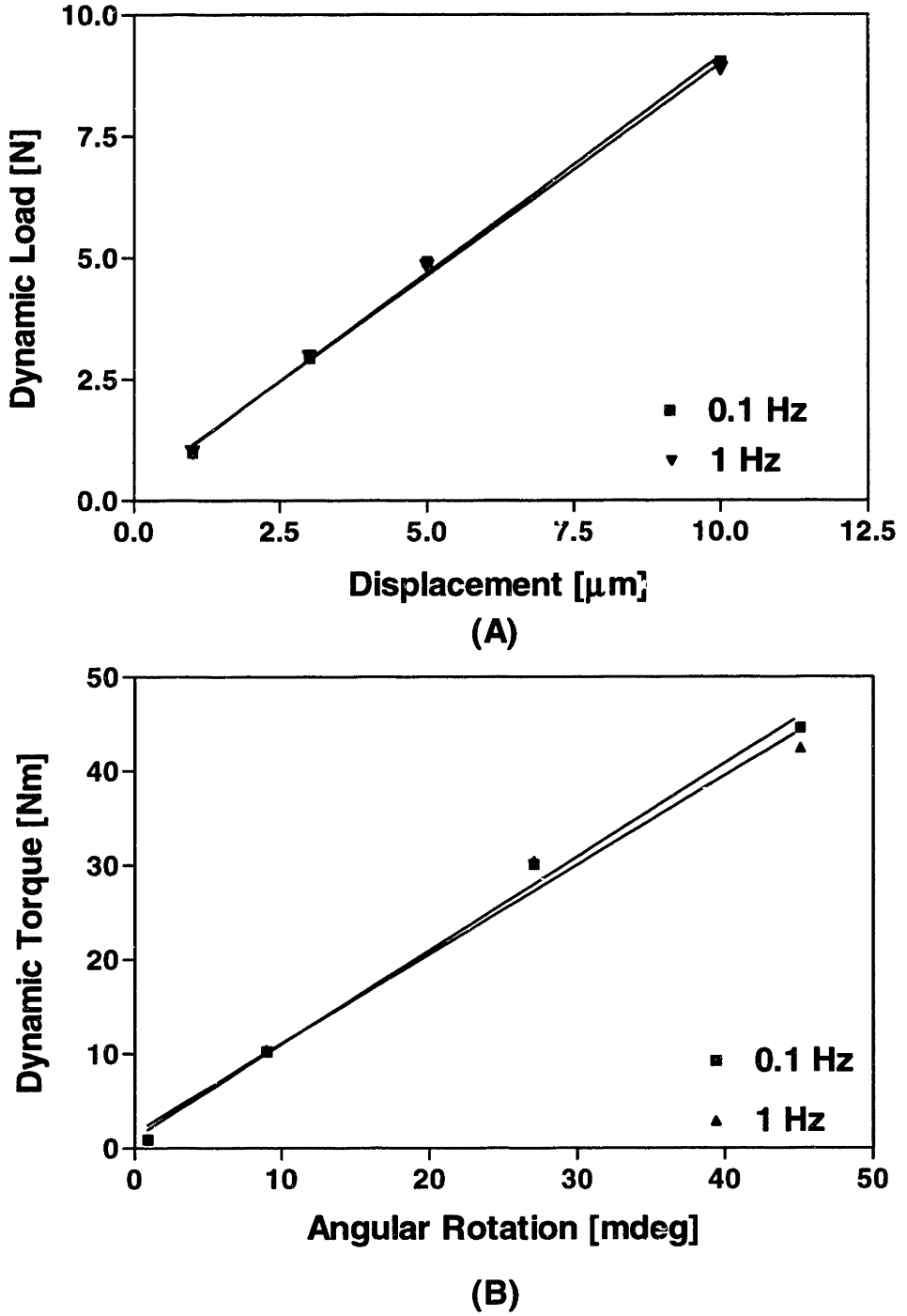

Figure 2-4: Axial force and torque were measured under 10 N compressive offset load, and different frequencies and strains. Axial and torsional compliances were calculated using linear regression (1.114 μm/N and 1.05 mdeg/Nm respectively).

The angle of deformational rotation on specimen, θ, is measured at the displacement of LVDT located 6.35 cm from the center of rotation, and torsional compliance of the machine is accounted for deformational rotation.

$$\theta = (LD - T \times \alpha)/D \tag{2.2}$$

where LD is the displacement at LVDT, T is the measured torque, α is the torsional compliance, and D is the distance to the LVDT from the center of rotation. The dynamic shear stress applied to the sample is computed from the recorded torque as

$$\tau = T \times R/I \tag{2.3}$$

where I is the polar moment of inertia of the area of specimen about the axis of the rotation, which is:

$$I = \pi R^4/2\ . \tag{2.4}$$

Finally, the effective shear modulus, G, is computed as

$$G = \tau/\gamma\ . \tag{2.5}$$

Simple Shear Mode

Cartilage specimens can be located at the chamber up to 12 samples, so shear modulus gives the average values of all samples. Shear strain in the samples is computed as the rotation angle (θ) times the circle radius (R) divided by sample thickness (h):

$$\gamma = \theta \times D/h \tag{2.6}$$

where θ is calculated like pure shear mode and D is the distance to LVDT from the center of rotation. The average dynamic shear stress applied to the samples is computed from the recorded torque as

$$\tau = T/(D \times A) \tag{2.7}$$

where T is the measured torque amplitude and A is the total sample area of all the disks. Finally, the effective shear modulus, G, of the cartilage disks is computed as

$$G = \tau/\gamma \, . \tag{2.8}$$

2.2.4 Axial Load and Torque Wave form: Example

Axial stress and shear stress wave form together with each strain are displayed in the following figures (Figure 2-5, Figure 2-6).

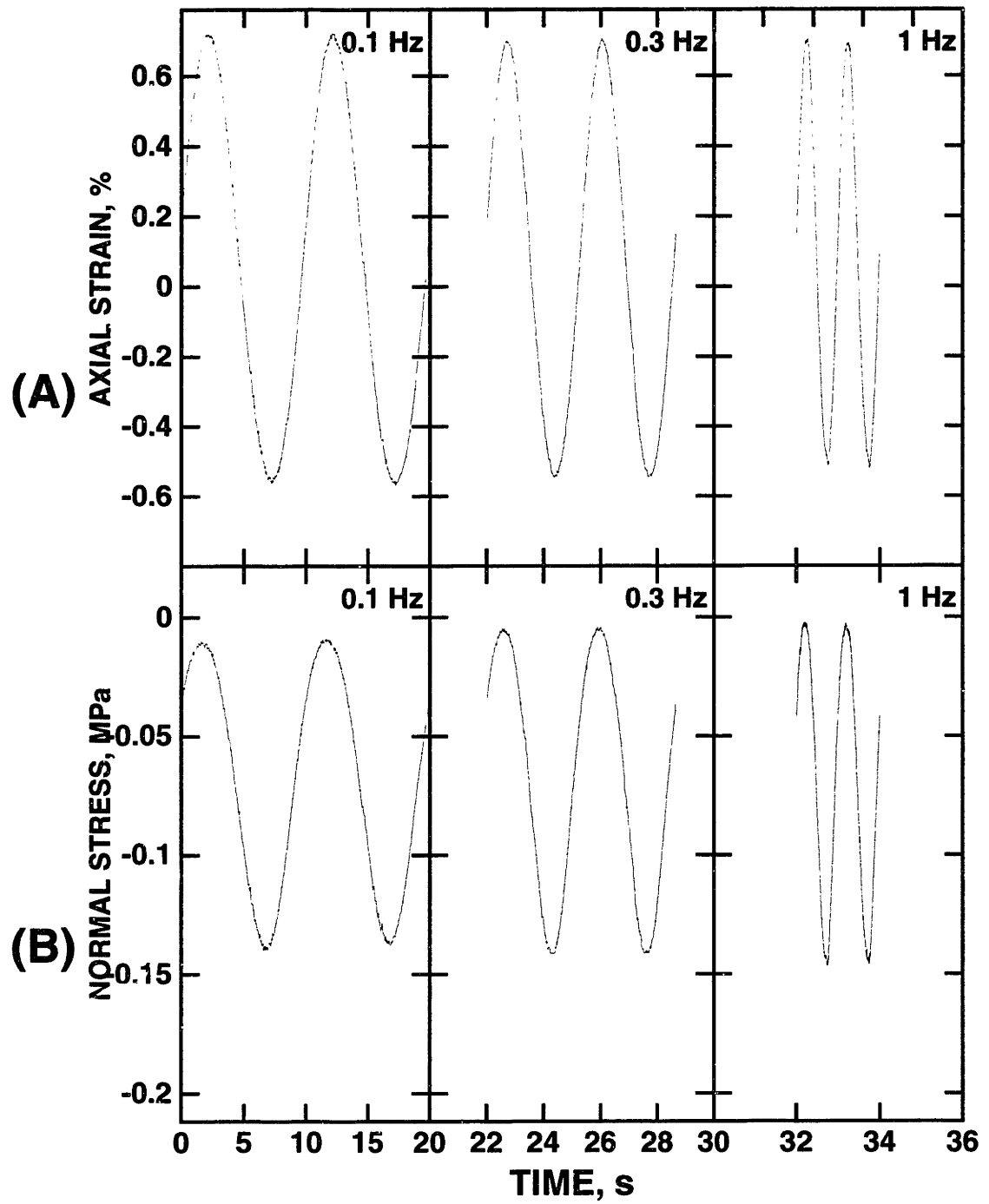

Figure 2-5: Examples of (A) applied sinusoidal axial strain, and (B) resulting stress waveforms at 0.1 Hz, 0.3 Hz and 1 Hz for 4 articular cartilage disks tested simultaneously in the dynamic chamber. The time axis is expanded in middle and right panels to show details. Normal stress waveform indicates an increase in axial modulus with increasing frequency.

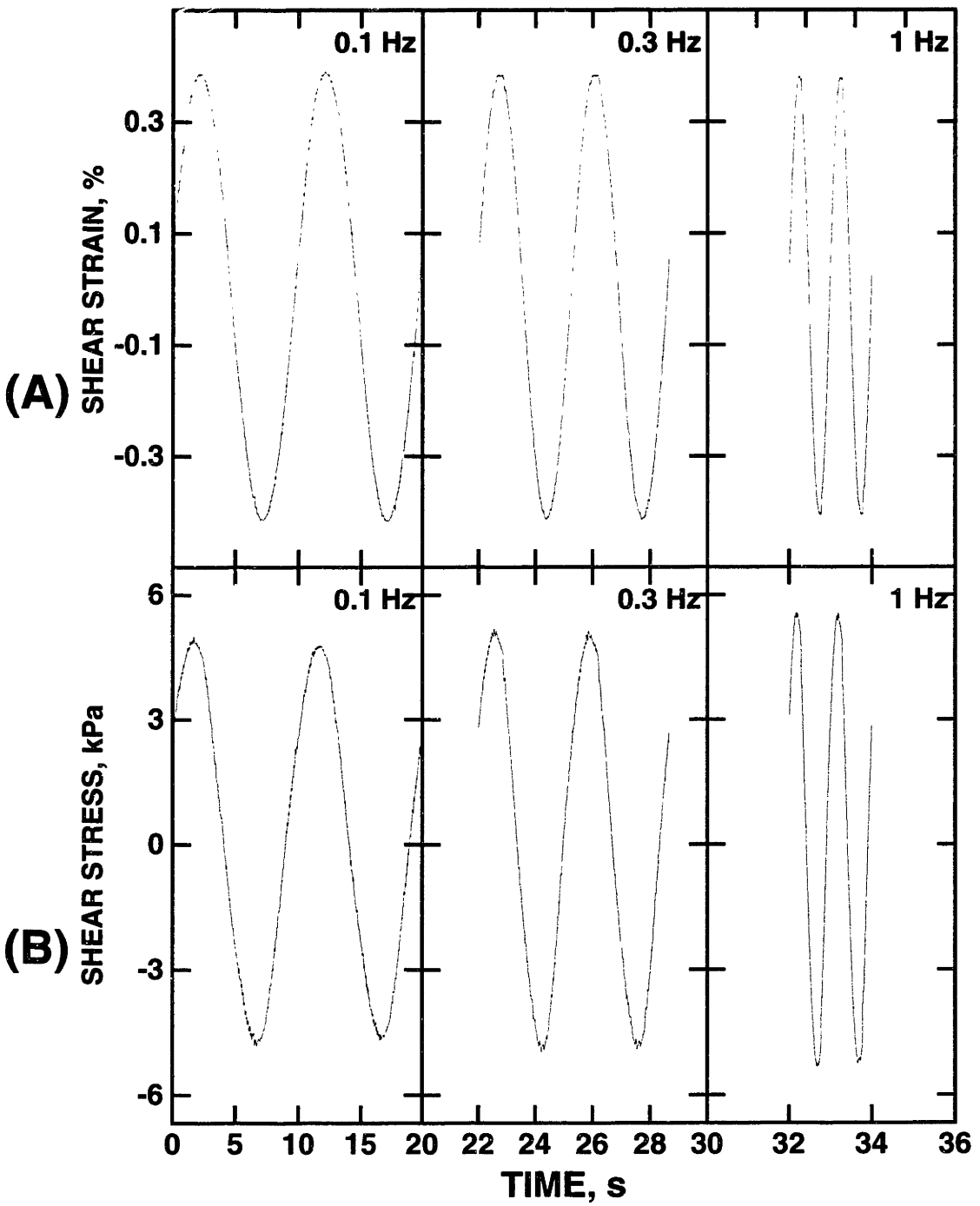

Figure 2-6: Examples of (A) applied sinusoidal shear strain, and (B) resulting stress waveforms at 0.1 Hz, 0.3 Hz and 1 Hz for 4 articular cartilage disks tested simultaneously in the dynamic shear chamber. The time axis is expanded in middle and right panels to show details. Shear stress waveform indicates an increase in shear modulus with increasing frequency.

Chapter 3

Mechanical Characteristics of Cartilage under Shear Strain

3.1 Introduction

Rheological behaviors of articular cartilage and hydrated biological tissues are derived from the complex interactions involving both the interstitial fluid and the extracellular matrix constituents such as negatively charged proteoglycan and collagen. Single phase viscoelastic model has been used to characterize the tissue behavior under creep and cyclic tests in torsion [21] and tension [52], and shear strain [44, 46, 55]. When the interaction between fluid and solid matrix is important like compressive deformation of soft connective tissue, poroelastic model has been adopted. Porous media are often described within the framework of continuum mixture theory where the medium is treated as the mixture of two different states, solid and fluid which occupy same physical space [8, 25]. Biot [3, 4] described equations of elasticity and consolidation for a porous elastic material containing fluid, and this view has been adopted in a homogeneous, isotropic, and poroelastic tissue case [11, 14, 27]. Levenston [28] remarked that under the assumptions of immiscible, nonreactive, isothermal, and quasistatic cases which are appropriate for hydrated biological descriptions, the mixture theory is mathematically equivalent to Biot's poroelastic theory [3].

Mechanical deformation accompanying volume change will induce a fluid motion, and this motion alters electrical and chemical condition of the matrix. But under pure shear strain, this deformation does not involve any volume change theoretically for the homogeneous and isotropic material, so the measured material behavior such as shear modulus can be mainly due to the intrinsic characteristics of collagen and proteoglycan. Hayes and Mockros [21] measured the shear properties of articular cartilage under torsional creep test, and compared the behavior of normal and degenerative tissue. Zhu et al [55] also investigated the shear properties of cartilage under the physiological range of frequency and pure shear condition, and tried to determine the relationships between the shear properties and the biochemical compositions of the tissue.

The molecular structure and stability, and mechanical function of collagen and aggregated proteoglycan in matrix are dependent on pH and ionic strength. Osmotic and electrostatic swelling pressure of articular cartilage and other hydrated tissue is due primarily to highly charged proteoglycan molecules [48, 17]. Eisenberg and Grodzinsky [11] developed an electromechanical model for charged and hydrated tissues to predict the kinetics of changes in swelling and compressive stress induced by changes in bath ionic strength. Also there have been several studies on the effect of ionic strength on the shear modulus of articular cartilage [38, 5].

In this study, the mechanical behaviors of cartilage under shear strain were investigated under different mechanical and physiological conditions. Dynamic shear modulus of cartilage was measured under different compressive offset, shear strain, and frequency of sinusoid. Also transient stress relaxation tests were performed to compare the peak and equilibrium shear modulus. Finally the effect of ionic strength on the dynamic shear modulus was investigated.

3.1.1 Viscoelastic Characteristics of Cartilage under Shear Strain

Viscoelastic characteristics can be described with the combined characteristics of solid and liquid. For elastic solid material case, stress is directly proportional to strain in small deformation limit, but insensitive to the rate of strain. Viscous liquid shows that the stress is proportional to the rate of strain, but independent of the strain itself. The descriptions above are limited to small deformation limit, and under finite strain the behavior of solids and liquids can not be explained by the above descriptions and it shows liquidlike and solidlike behaviors. But a viscoelastic material shows those combined behavior even if both strain and rate of strain are infinitesimal. When such materials are subjected to sinusoidal strain, the stress is neither exactly in phase with the strain, like perfectly elastic solid, nor 90 degree out of phase, like perfectly viscous liquid, but is somewhere between [13]. This phase difference shows that some of the deformational energy is stored and recovered in each cycle, and also some of it is dissipated as heat.

Viscoelastic behavior of articular cartilage was measured under pure shear, or simple shear strain less than 3%. Under infinitesimal shear strain, the mechanical behavior of cartilage can be described as flow-independent characteristics, since there will be little or no dilatation or compaction of matrix, and thus negligible fluid flow into or out of the matrix [46].

3.2 Methods

3.2.1 Specimen Preparation

Cartilage disks (8.4 mm for pure shear mode and 3 mm diameter for simple shear mode experiments, by 1 to 1.2 mm thickness) were prepared using same protocol explained in 4.2.2. 8.4 mm diameter specimens were punched out of 9.4 mm slices using a dermal punch.

3.2.2 Experimental Protocol

For simple shear mode experiments, matched cartilage disks from a single anatomical site (4 at a time) were subjected to cyclic shear deformation (0.01 - 1 Hz) at nominal engineering shear strain of 0.5-2.0%, or for transient stress relaxation experiment, shear strain is increased up to 3% incrementally. The center of 8.4 mm sample was aligned with the axis of rotation for pure shear mode experiments.

Shear modulus behavior under different mechanical conditions: Shear modulus was measured under different compressive offset, shear strain, and frequencies. Except for measurements under different ionic strengths, all experiments were performed in the same chemical components, temperature, and air components of the bath media before and during the experiments.

Shear modulus behavior under different ionic concentration: Shear modulus was measured under 20% compressive offset, 1 Hz frequency and 0.9, 1.2, and 1.5% three different shear strains of sinusoid at simple shear mode. Four 3 mm disks, which were out of a single anatomical site of 9.4 mm disk, were used for the measurement. Samples were first moved to 0.15 M NaCl solution, washed twice over 20 minutes, and then moved to the dynamic shear chamber in the incubator. 600 μl of NaCl solution were added to each specimens in the incubator without changing the axial position of the upper chamber. $\sim$10 minutes were used for the chemical and mechanical equilibrium between sample and solution and the shear modulus was measured after that. For some experiments both shear modulus and axial stiffness were measured. Also to measure the extracted GAG content, after measuring the axial or shear modulus, the bath solution was transferred to 24 well dish from the chamber. 20 μl of solution at different ionic concentration was taken for the GAG assay (Section 4.2.4). To remove the other effects like pH and temperature on the shear properties, the bath pH was maintained within the range of pH 6-8 and bath temperature was equilibrated with that of incubator.

3.3 Results

3.3.1 Shear Modulus under Different Mechanical Conditions at PSM

Figure 3-1 shows the phase difference between torque and angular displacement, which is consistent with a flow-independent viscoelastic characteristics, and typical behavior of shear modulus under different frequencies and shear strains. Shear modulus was increased under increasing frequency in the range of 0.1-1 Hz, and interestingly shear modulus was decreased under increasing shear strain (Figure 3-2). The articular cartilage exhibited an intrinsic time dependent stress relaxation behavior upon the instant application of a shear strain (0.5% shear strain/sec) (Figure 3-3). Equilibrium shear modulus was nearly linear to the applied shear strain magnitude (slope = 0.207 MPa), but peak stress showed a nonlinear dependence on the magnitude of shear strain.

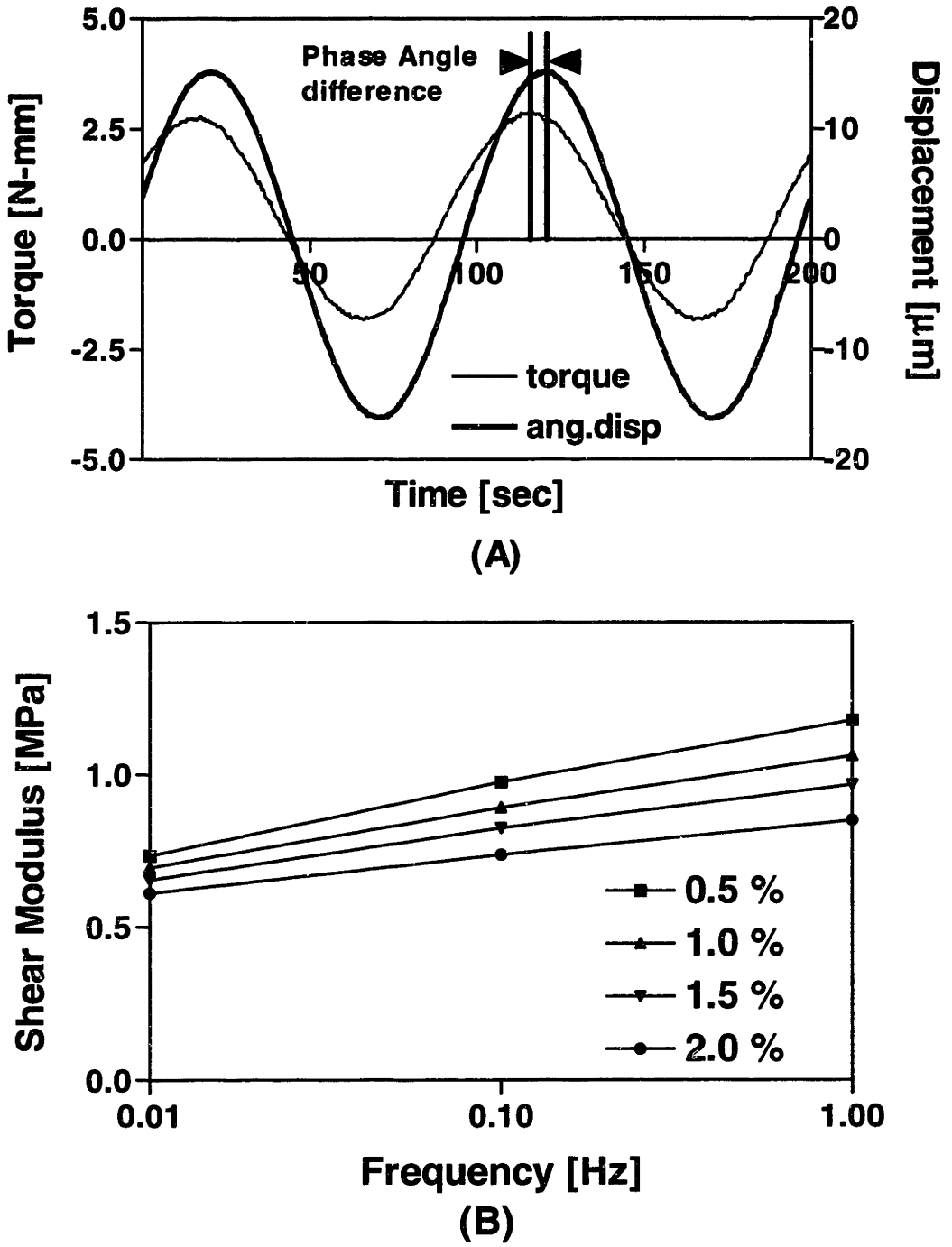

Figure 3-1: Viscoelastic behavior of cartilage under shear strain. (A) shows the phase difference between torque and angular displacement and (B) shows the frequency dependence of the shear modulus.

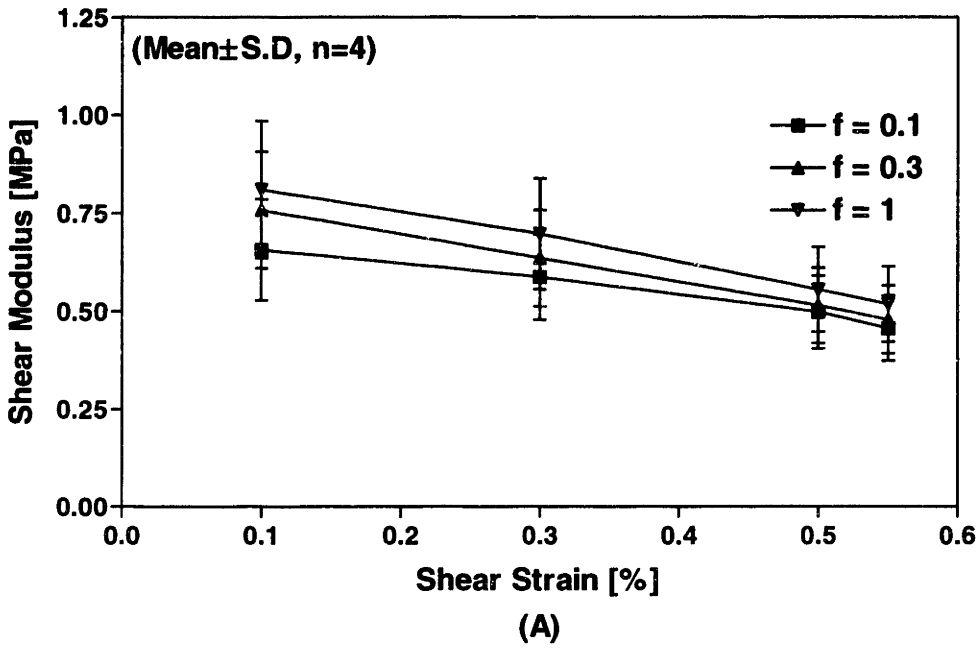

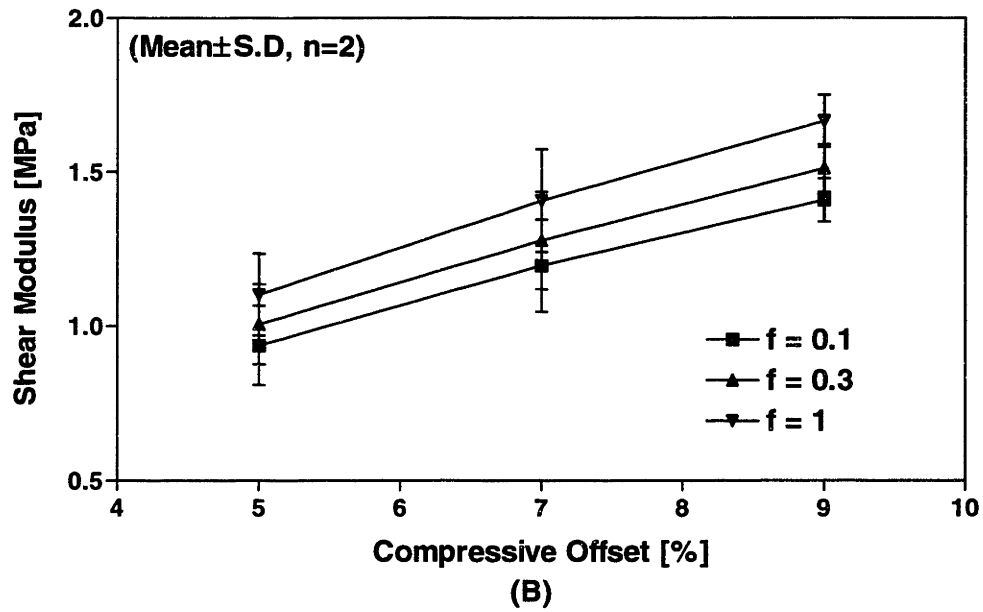

Figure 3-2: Shear modulus is increased under increasing frequencies and compressive offset, but the increase in the shear strain decreased the shear modulus. At (A), 7% compressive offset and at (B), 5% Shear strain were used for the measurement.

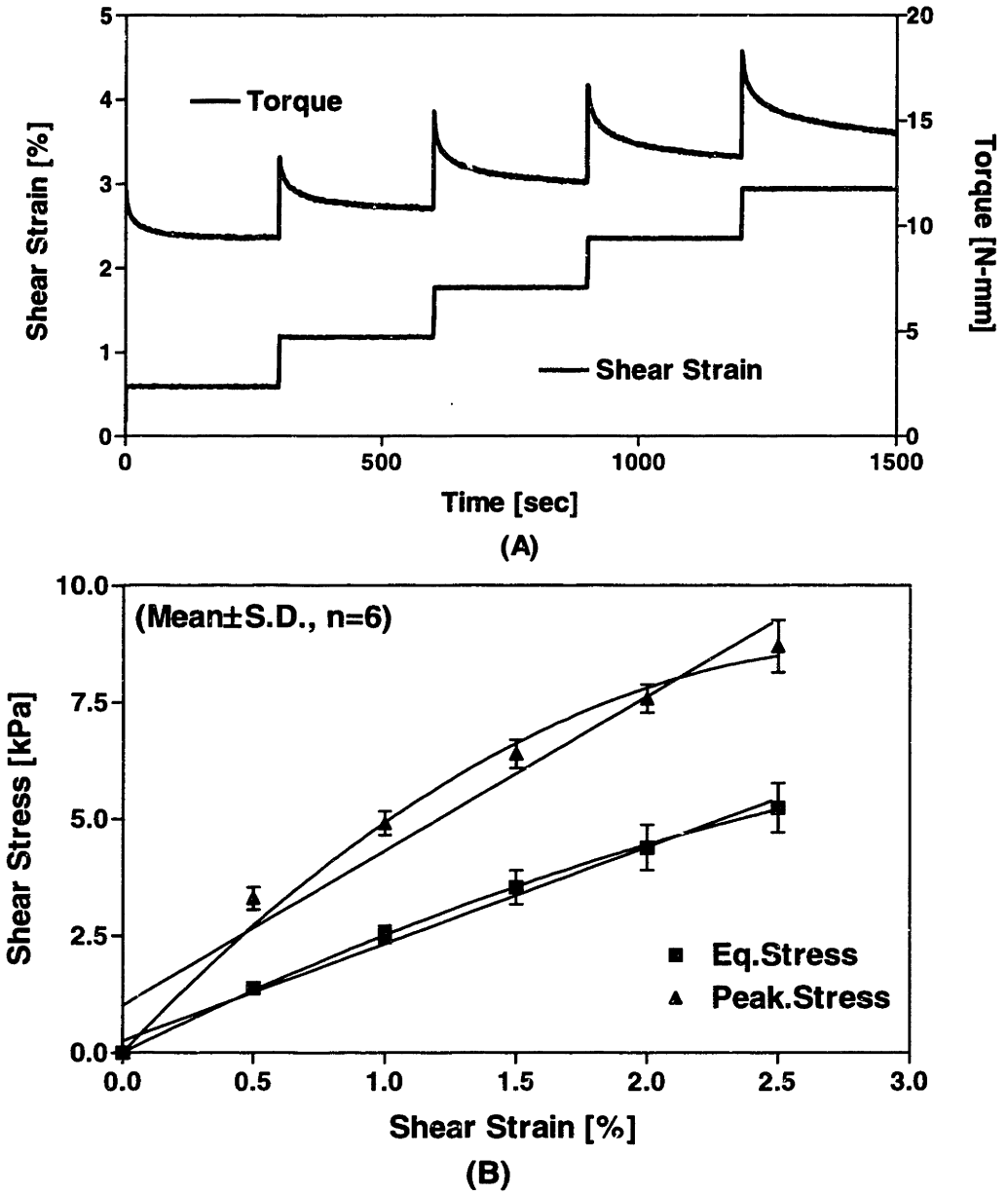

Figure 3-3: A. Cartilage exhibited an intrinsic time dependent stress relaxation behavior upon the application of shear strain. B. Linear and 2nd polynomial regression curve were represented together with the data. The peak stress showed a nonlinear behavior to the applied shear strain, but the equilibrium stress showed $r^2 = 0.99$ goodness of fit to the linear regression curve and the slope of the curve was 0.207 MPa.

3.3.2 Shear Modulus under Different Ionic Strengths at SSM

Shear modulus was measured at 0.9%, 1.2%, and 1.5% shear strain, and Figure 3-4 shows the experimental procedure. To check whether the shear modulus behavior was dependent on time, the shear modulus was measured again at same concentration during sequential segments of the experiment in which ionic strength was both increasing and decreasing.

Shear modulus decreased with increasing ionic strength up to 1.0 M NaCl concentration, but began to increase above $\sim$ 1.0 M. Above this concentration GAG was extracted out of tissue to the bath (Figure 3-8). Once the bath concentration reached $\sim$ 1.0 M ionic strength, the shear modulus showed strong time-dependent behavior and it did not reproduce the typical behavior before the bath concentration was increased up to 1.0 M NaCl (Figure 3-5) due to the GAG extraction. To compare the behavior of shear modulus under different bath concentration with that of axial modulus, axial modulus and shear modulus both were measured for some of samples. The axial modulus decreased monotonically with increasing bath concentrations within the range of ionic concentrations used.

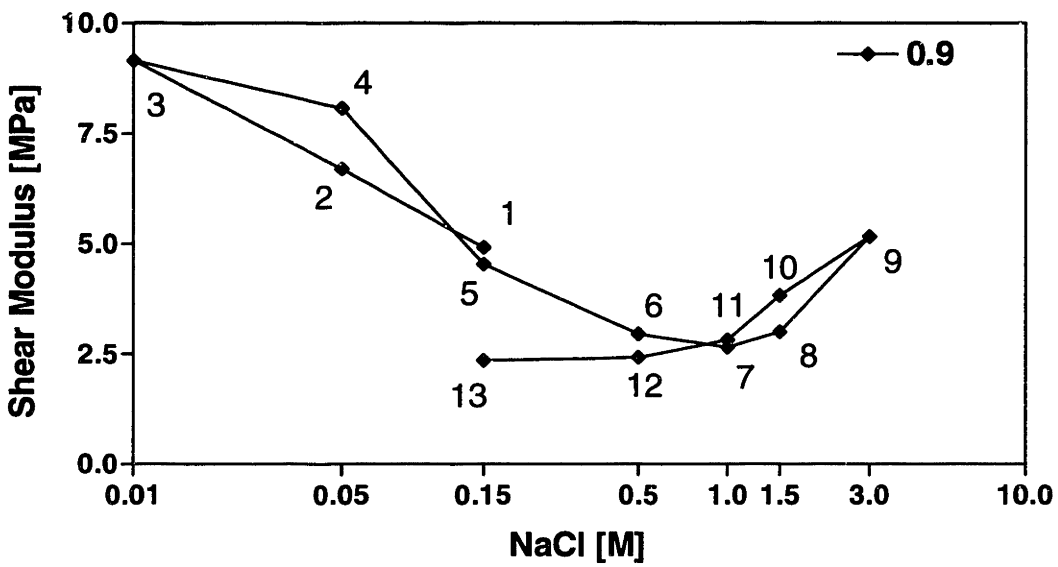

Figure 3-4: Experimental procedure: cartilage specimens were first equilibrated with 0.15 M NaCl solution and the concentration was decreased to 0.01 M, and back to 0.15 M and then increased up to 3 M, and finally back to 0.15 M NaCl. Above ~1 M, proteoglycan extracted out of tissue and shear modulus did not show the behavior before the ionic strength was increased up to 1 M NaCl.

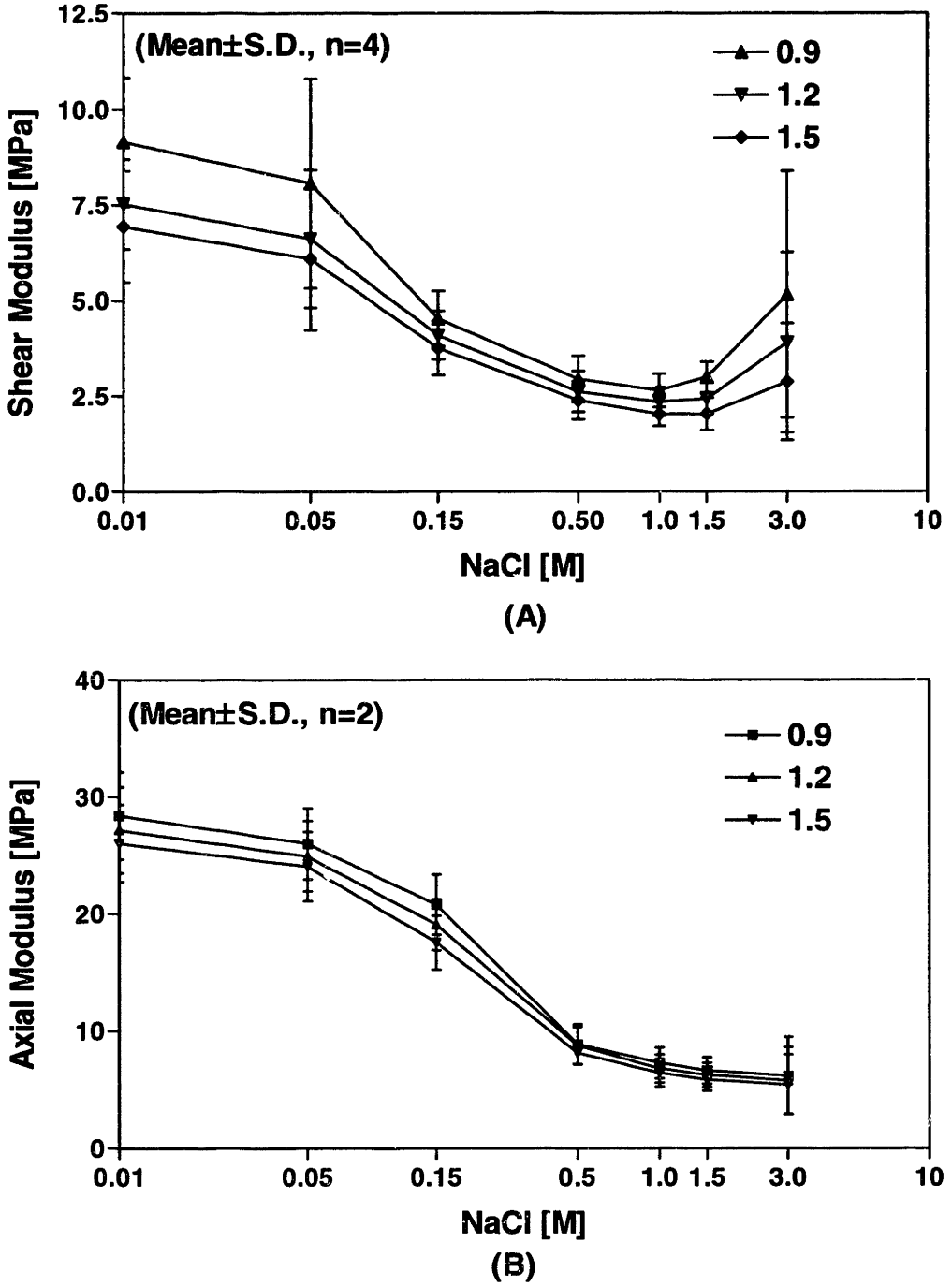

Figure 3-5: A. Shear moduli decreased up to 1.0 M under increasing ionic concentration and began to increase above 1.0 M NaCl concentration. B. Axial moduli decreased monotonically under increasing ionic strength.

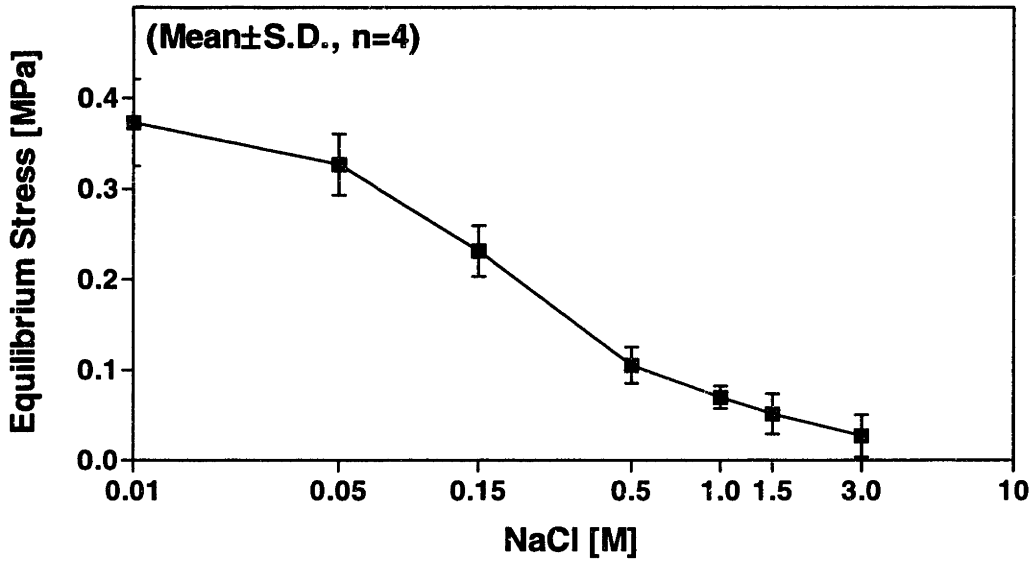

Figure 3-6: Static load decreased under increasing ionic strength.

The equilibrium static load was recorded (Figure 3-6), and static stress was monotonically decreased under increasing ionic strength.

To see the behavior in axial modulus and shear modulus was related with equilibrium static stress, the axial modulus and shear modulus was represented regarding to static stress (Figure 3-7).

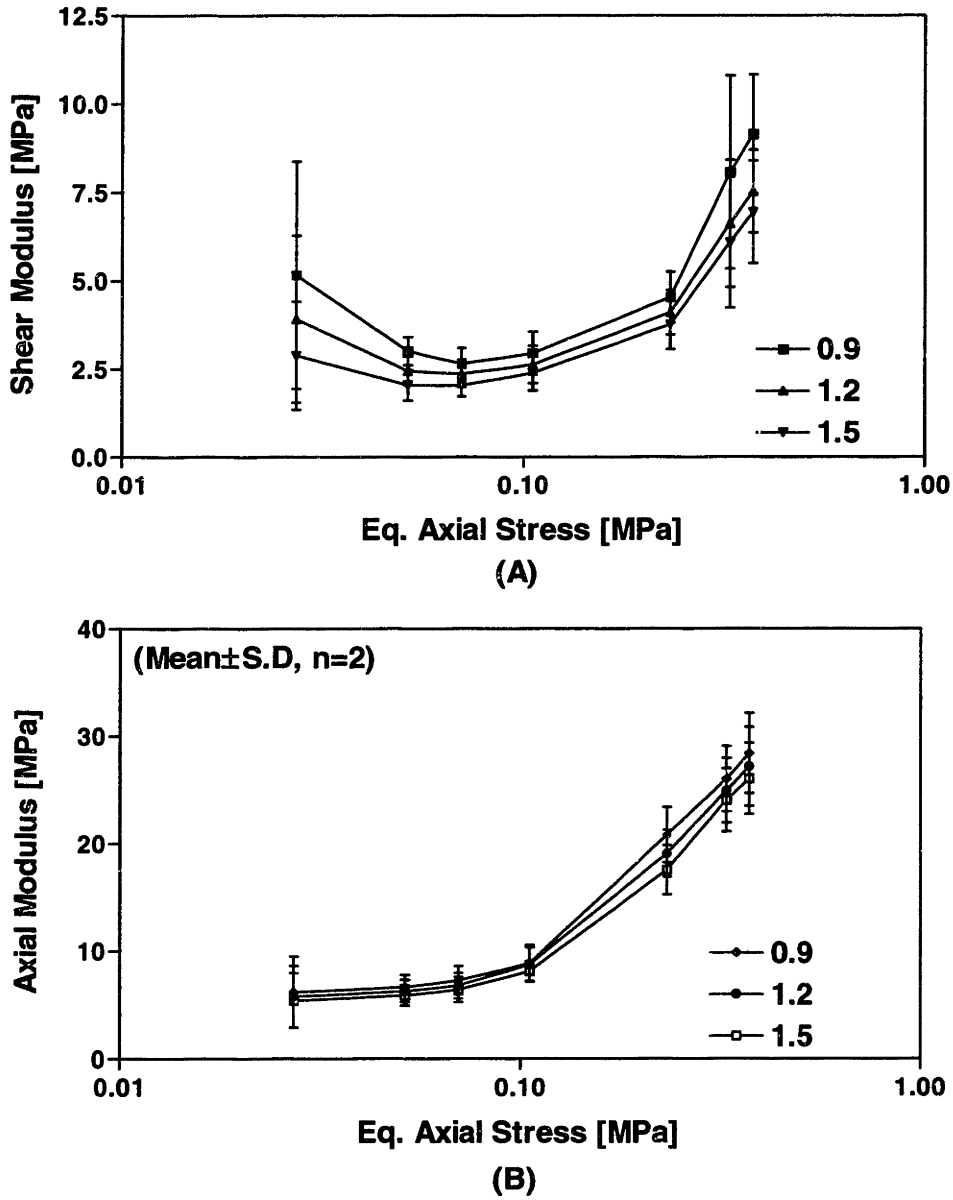

Figure 3-7: Above 1.0 M NaCl concentration, shear modulus increased even if static compressive load was decreased. Axial modulus behavior is directly related with the equilibrium static load.

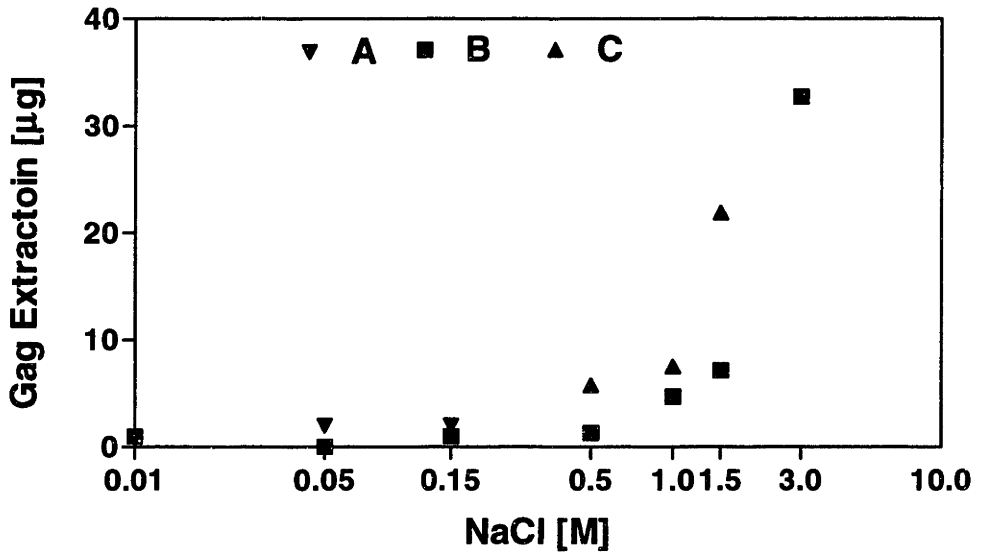

Figure 3-8: A, B, and C correspond to 1 and 2, 3 to 9, and 10 to 13 of experimental procedure, respectively. Refer to Figure 3-4.

3.4 Discussion

The dynamic shear properties of cartilage were determined in pure shear and simple shear mode under different mechanical conditions and bath ionic concentration. Under pure shear mode, the shear modulus was measured at different frequencies (0.01-1 Hz), compressive offset (5, 7, and 9%), and up to 1% shear strain. As previously reported [21, 20, 52], the cartilage exhibited viscoelastic behavior in shear strain. Interestingly, strain softening of cartilage was observed under increasing shear strain; this softening effect was briefly mentioned by Simon [44], and Zhu [54] reported this effect in meniscus and mentioned that this may be due to the relative sliding motion of collagen fibers and proteoglycans in the matrix of the meniscus. The result of transient relaxation measurement of cartilage under shear strain showed that the peak stress is nonlinear with the applied shear strain, and the equilibrium stress is nearly linear with the shear strain. So it can be assumed that the softening effect of cartilage under shear strain is related with the transient elastic behavior, because peak stress corresponds to the transient elastic behavior of matrix. The phase difference between stress and strain implied that some of the deformational energy is dissipated as an another form like heat. In this experiment the phase difference was in the range of 5-25 degree depending on the shear strain, frequency, and compressive offset. Previous studies have shown that the phase difference in collagenous tissue like ligaments is ~3.6 degree [51], and for the proteoglycan network in solution the phase difference is in the range of 50-70 degree depending on the proteoglycan structure and solution concentration [32]. So the phase difference in articular cartilage can be assumed to be due to both proteoglycan and collagen. Researchers [55] have explained the energy dissipation in cartilage is related with several mechanisms such as the interaction between proteoglycan and water, collagen and water, proteoglycan and proteoglycan, proteoglycan and collagen, and internal viscous dissipation within the fluid. In the shear strain deformation of articular cartilage which involves little or no volumetric deformation, or relative fluid motion, the energy dissipation is likely due to proteoglycan-proteoglycan or proteoglycan-collagen interaction.

The shear properties of articular cartilage were investigated under different ionic concentrations in the range of 0.01-3.0 M. Shear modulus was decreased as a result of increasing ionic strength up to ~1.0 M NaCl concentration in bath, and after that shear modulus was increased. On the contrary axial modulus was decreased monotonically under increasing ionic strength up to 3.0 M bath concentration. Measured axial equilibrium stress showed similar trends to the axial modulus behavior. The initial softening of articular cartilage under shear strain as a result of increased ionic strength up to 1.0 M can be explained by either the reduction of repulsion forces between proteoglycan due to the screening effect of increased mobile ions, or decreased osmotic pressure due to increased mobile ions in a media solution. The stiffening of shear modulus beyond 1 M NaCl concentration was previously reported by Bodine [5], and he proposed this effect may be due to the dehydration in collagen network which resulted in the reduction in the plasticizing effect of water, or the anti-platicizer effect of NaCl ions. Even if the reason of stiffening is not clear, but there will be a conformational change in collagen and proteoglycan structure under higher bath ionic concentrations, and also GAG began to be extracted out of matrix beyond 1 M NaCl (Figure 3-8).

Chapter 4

Biosynthetic Response of Chondrocytes under Tissue Shear Strain

4.1 Introduction

The extracellular matrix of cartilage is maintained and produced by chondrocytes, and physical environment affects the metabolism of chondrocytes via cell deformation, changes in hydrostatic pressure, induced fluid flow, and changes in chemical environment. However relative contributions among those changes in mechanical and physicochemical environment are unknown, and researchers tried to separately investigate the effect of one of those factors on the biosynthetic response of chondrocytes.

Various loading-induced physical phenomena (fluid pressure, cell/matrix deformation, streaming potential, etc.) have been proposed to play different roles in metabolic regulation [16, 18]. Cyclic hydrostatic pressure in the physiological ranges, 5 MPa $\sim$ 15 MPa, was reported to stimulate matrix synthesis in cartilage [19, 37], and Sah et al [41] reported that dynamic axial compression of appropriate range of frequency and amplitude increased the biosynthetic response of chondrocytes. Smith et al [45] applied fluid-induced shear on monolayer culture of articular chondrocytes

and found that it stimulated GAG synthesis and increased the length of newly synthesized chains in human and bovine chondrocytes. Ionic and osmotic environment also affected matrix synthesis rates articular cartilage [47].

However most of mechanical deformation involves intratissue fluid motion, and the fluid motion changes physicochemical and electrical environment due to the separation of mobile ions from negatively charged fixed ions in matrix (Figure 4-1).

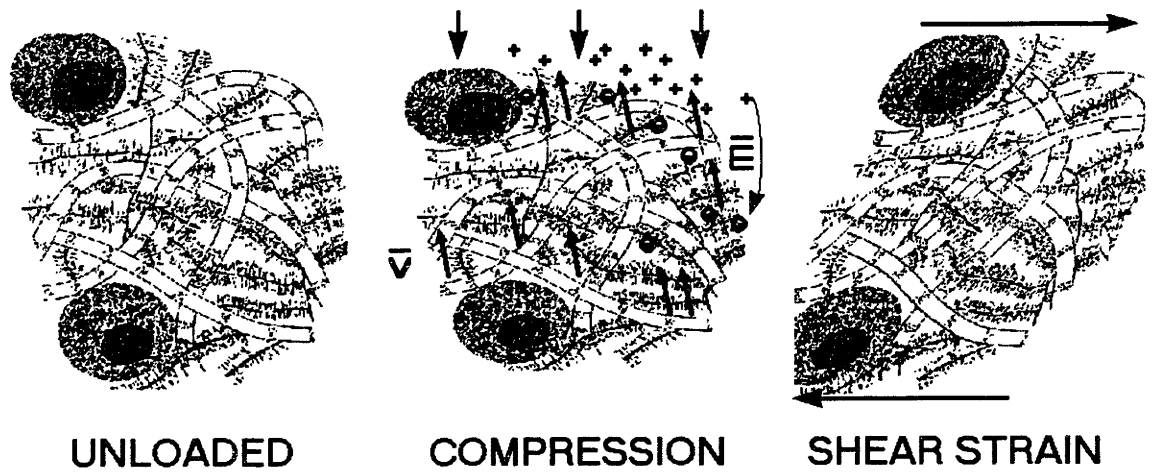

Figure 4-1: Three different states of cartilage. When cartilage is axially deformed, relative fluid motion induces streaming potential and changes electric field (B). In contrast, when cartilage is deformed by shear strain, no relative fluid motion is involved(C).

Similarly changes in physicochemical and electrical environment induce mechanical deformation in matrix. In contrast, macroscopic tissue shear strain of a poroelastic tissue such as articular cartilage does not involve volumetric changes, intratissue fluid motion, or pressure gradients, and can decouple the effect of mechanical deformation from other effects on chondrocytes metabolism.

Figure 4-2 shows the schematic configuration of a machine and the mechanism of shear strain application. In this study simple shear strain is applied to tissue samples, so a relative fluid motion can be induced near the leading and trailing edge

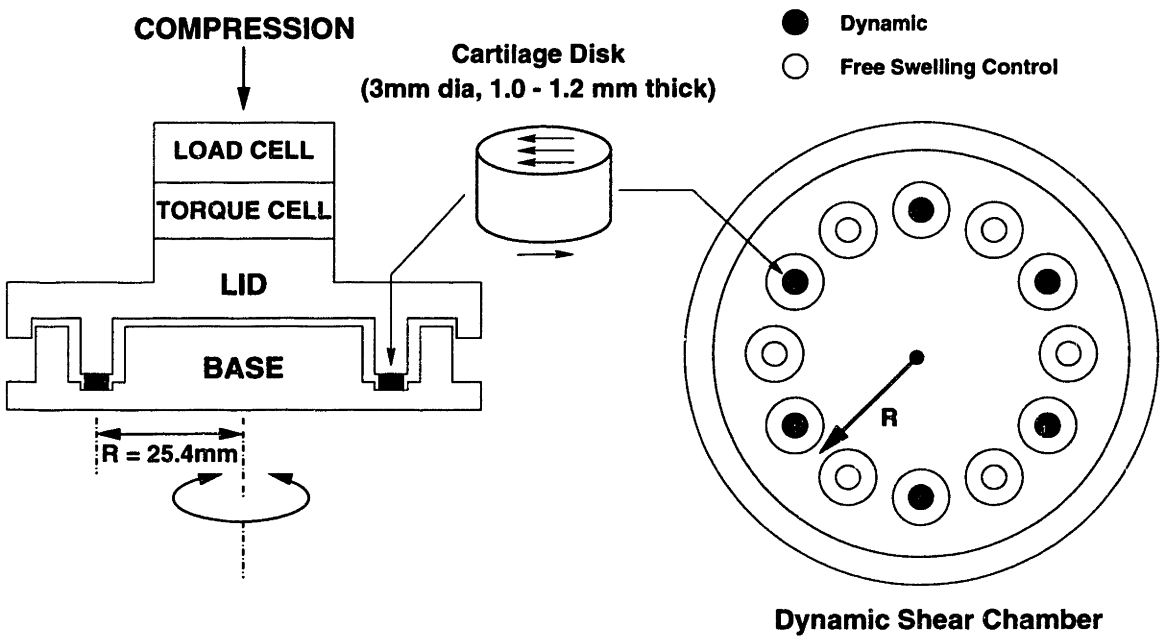

Figure 4-2: Cartilage explants are placed in wells in the base of an autoclavable polysulphone chamber. The platens of the nonrotating lid compress the cartilage. The platens surfaces were roughened, but no adhesives were used in culture experiments involving shear deformation. Since the lid has only 6 platens, 6 out of 12 plug were loaded while another 6 plugs in the alternate wells were unloaded controls.

to satisfy momentum balance. To check the possibility of local stimulation by fluid flow, 2 mm core out of 3 mm disk was separated and the incorporation rate in core and outer ring region was compared.

4.2 Materials and Methods

4.2.1 Materials

Dulbecco's modified Eagle's medium (DMEM low glucose), Dulbecco's phosphate buffered saline (PBS), L-ascorbic acid from Gibco, Grand Island, NY. Nonessential amino acids, sodium sulfate, L-proline, shark chondroitin sulfate, and protease-K, and gentamycin sulfate were from Sigma, St. Louis, MO. Sodium ^{35}S-sulfate was from New England Nuclear, Boston, MA. L-5-^{3}H-proline was from Amersham, Arlington Heights, IL. ScintiVerse Bio-HP scintillation fluid from Fisher, Boston, MA. Semimicro polystyrene cuvettes and 24, 96 well plates from VWR, Boston, MA. Acrylic cuvettes were from Sarstedt, Pennsauken, NJ. Dimethylmethylene blue dye was from Polysciences, Warrington, PA, and Hoechst 33258 DNA dye was from Hoefer-Scientific Instruments, San Francisco, CA.

4.2.2 Sample Preparation

Cartilage tissue was obtained from articular cartilage at femoropatellar groove of one to two weeks old calf from a local abattoir (A.Arene, Hopkinton, MA) immediately after slaughter. Four to five cylindrical cores, 9.5 mm diameter and $\sim$ 15 mm thickness, of cartilage and underlying bone were drilled from medial and lateral site of femoropatellar groove. Each cartilage-bone cylinder was inserted into the sample holder of a sledge microtome (Model 860, American Optical, Buffalo, NY), and the superficial tissue of it was removed until a flat surface was achieved. Then the next two 1 $\sim$ 1.1 mm thickness cartilage slices were removed and placed with $\sim$ 1 ml PBS with antibiotics (50 μg/ml gentamycin). From one slice, four 3 mm diameter disks were punched using dermal punches (Miltex Instruments, Lake Success, NY) (Fig-

ure 4-3). During the harvesting process, cartilage was kept moist by frequent rinsing with sterile PBS supplemented with antibiotics.

After 3 mm diameter, 1 mm thickness disks were prepared, the cartilage disks were incubated in media (DMEM with 10mM HEPES, 10 % FBS, 0.1mM nonessential amino acids, an additional 0.4 mM proline, 20 μg/ml ascorbate, and 50μg/ml gentamycin) at 37 °C in 5 % CO_2 and 95 % air. The total time from slaughter to incubation was less than 8 hours. The media was changed daily, and after 2-6 days of culture, disks were subjected to different protocols.

4.2.3 Experimental Protocol

Four 3 mm diameter plugs out of one 9.5 mm diameter disk were distributed in each of four test conditions: Dynamic shear, free swelling control in Dynamic shear chamber, and static and free swelling control in Static chamber (Figure 4-3). To apply dynamic shear strain, a 10% compressive offset was first applied. Therefore the static control plugs were also maintained at 10% offset compression. 0.1 Hz, 1% sinusoidal shear strain was applied to cartilage specimens. During 24 hour loading, cartilage disks in each well were radiolabeled with ^{3}H-proline and $^{35}SO_4$-sulfate for measuring synthesis of protein and proteoglycan.

Spatial localization of biosynthesis

For one experimental series (N=6), a 2 mm diameter core was separated using a dermal punch from each 3 mm dynamic and static control disks and analyzed separately from the remaining annular ring [24].

4.2.4 Biochemical Analysis

Unincorporated radiolabeled media Washing: After application of appropriate loading, free-label in cartilage was removed by serially washing samples three times over 1 hour in 1 ml PBS (without Calcium and Magnesium) supplemented with

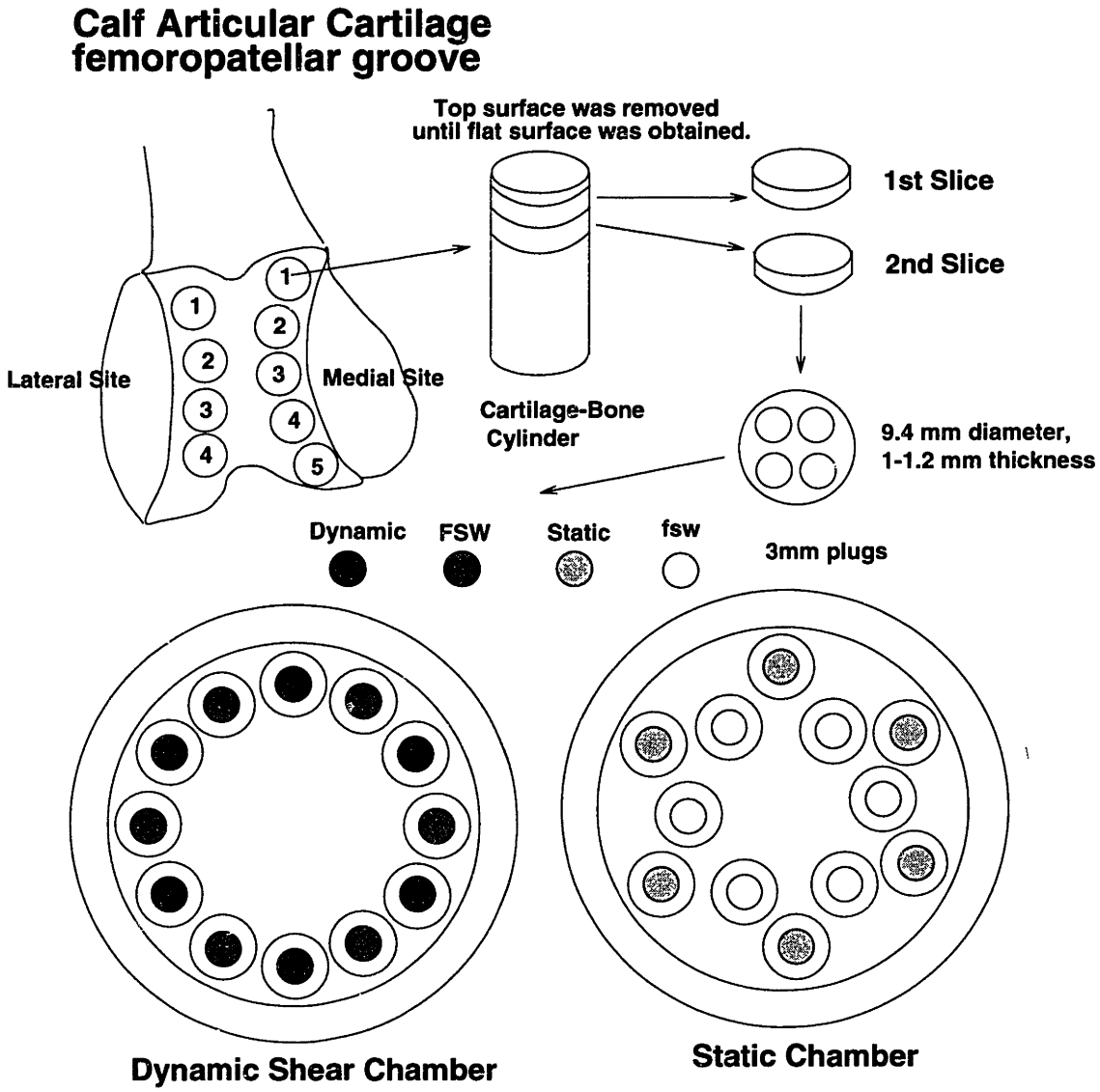

Figure 4-3: Cartilage tissue was obtained at femoropatellar groove of calf articular cartilage. Anatomically matched four 3 mm diameter, 1 $\sim$ 1.2 mm thickness plugs are distributed in four different conditions: Dynamic shear (Dynamic), free swelling control (FSW) in dynamic shear chamber, static control (Static), free swelling control (fsw) in static control chamber.

0.8 mM sodium sulfate and 0.5 mM L-proline at 4°C.

Protease K Digestion: All samples were solubilized in 1.0 ml protease K (100μg/ml in 50 mM Tris-HCl, and 1 mM $CaCl_2$, pH 8.0) for 12 $\sim$ 18 hours at 60 °C water bath. For core vs. ring experiments, 0.5 ml of protease K solution was used for core and ring each.

β Counting: 100μl of protease K digests were taken and mixed with 2ml of Scintillation fluid. The samples were counted on an RackBeta 1211 counter (Pharmacia LKB Nuclear, Turku, Finland) and the counts were corrected for spillover.

GAG Assay: 100μl of digests were mixed with dimethylmethylene blue (DMMB) dye solution in a semimicro polystyrene cuvette. The absorbance of 525 nm was measured using a spectrophometer (Model 3B, Perkin Elmer, Norwalk, CT). For small quantity of GAG molecules, 20μl of digests were mixed with DMMB dye and the absorbance at 520 nm was measured using a microplate reader (Vmax microplate reader, Molecular Devices, Menlo Park, CA). Shark chondroitin sulfate was used as standards [12].

DNA Assay: 100μl of digests were analyzed for DNA content using the Hoechst 33258 dye. The samples were mixed with 2 ml of the dye in an acrylic cuvette and the fluorescence was measured using a spectrofluorometer (SPF 500C, SLM Instruments, Urbana, IL) [23].

4.2.5 Statistics

Groups were compared using paired t-tests with a significance level of $p < 0.05$.

4.3 Results

4.3.1 Biosynthetic Response

The incorporation rate in dynamically sheared disks was compared to the incorporation rate in free swelling control and static control. To make the temperature of two chambers to be equal, since the rotating table conducts a heat generated by a

driving motor, thermostat was attached to the top of the table, and the temperature on the table and ambient air near static chamber were compared. In addition to the temperature control for the incubator, coolant water tube was wrapped around motor and the temperature of the table was indirectly controlled by adjusting the temperature of coolant water. To check the pseudo effect which might be induced by other than control factors, such as temperature difference between two chambers or systematic errors due to two different chambers being used, the incorporation rate in each free swelling group, FSW and fsw, were compared. Both ^{35}S-sulfate and ^{3}H-proline incorporation in dynamically sheared disks were significantly higher ($p < 0.001$) by 25% and 41%, respectively, than in control disks held at the same static offset compression (Figure 4-4). Unloaded free-swelling controls in adjacent wells of chamber showed incorporation rates of ^{35}S-sulfate (42 ± 16 pmole/μg DNA/hour) and ^{3}H-proline (82 ± 23 pmole/μg DNA/hour) that were comparable to previous results [41] and not significantly different from statically compressed controls.

4.3.2 Spatial Localization

To check the possibility of local stimulation effect by relative fluid motion in the outer edge, the incorporation rate in 2 mm core and outer ring was compared (Figure 4-5), since under axial dynamic compression, the incorporation rate in the outer ring was bigger than that of core region due to possibly the induced fluid effect [24]. The incorporation rate was normalized by the incorporation rate of free swelling control group. It showed that the increase in the incorporation rates was similar between core and ring compared to the incorporation rate in free swelling control. The incorporation rate of ^{3}H-proline and ^{35}S-sulfate in core and ring of dynamic group was increased by $\sim$ 30% over free swelling control. Also the incorporation rate of core and ring in static control was not different from that of free swelling control.

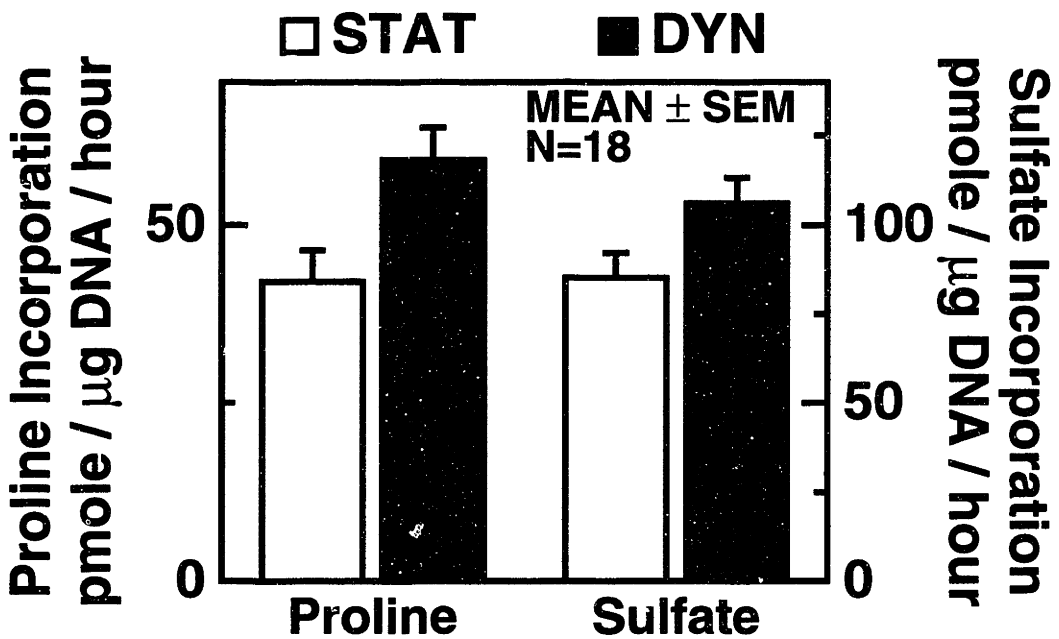

Figure 4-4: ^{35}S-sulfate and ^{3}H-proline incorporation in dynamically sheared (solid bars) and statically compressed (open bars) disks. Incorporation in dynamically sheared disks was significantly higher ($p<0.001$) than in static control disks.

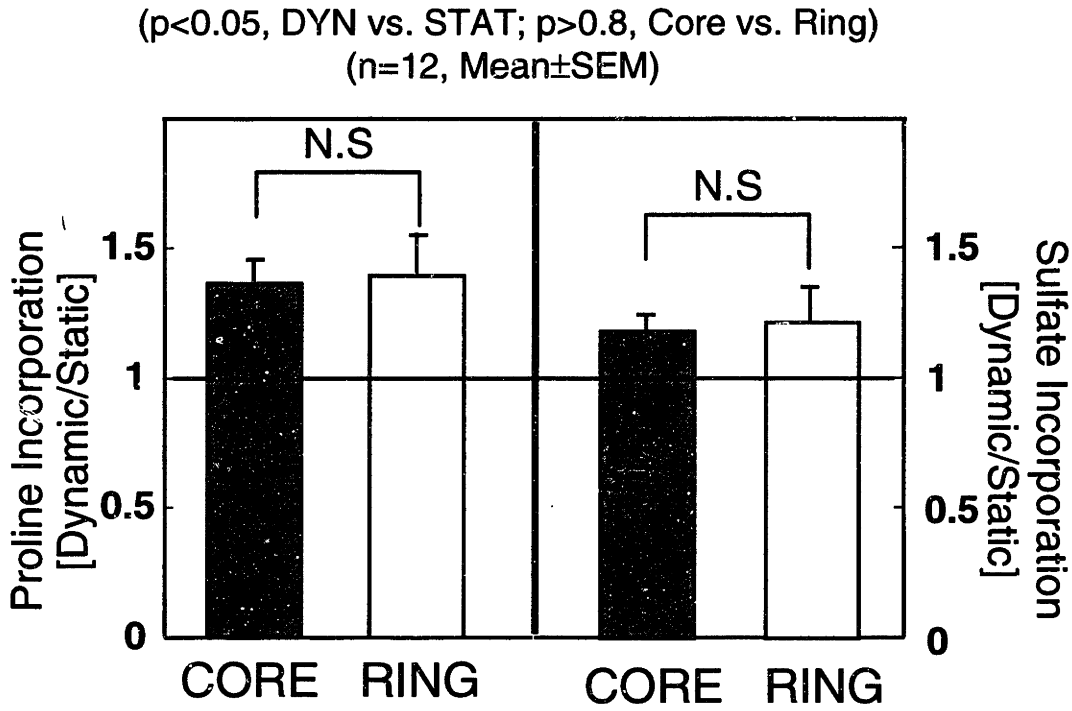

Figure 4-5: Comparison of ^{35}S-sulfate and ^{3}H-proline incorporation in Core vs. Ring of dynamically sheared and statically compressed disks. The incorporation rates in dynamic group were normalized to the average of the incorporation rate in static group which is represented as "1" in this figure. Protein and proteoglycan synthesis in core and ring of dynamically sheared disks were significantly increased over statically compressed disks.

4.3.3 Change in Mechanical Property of Cartilage during Shear Deformation

During 24 h loading, the average amplitude of torque during 4 cycle was recorded at every 30 minutes. Figure 4-6 shows the typical behavior of shear modulus change. Shear modulus decreased initially and after that reached a plateau.

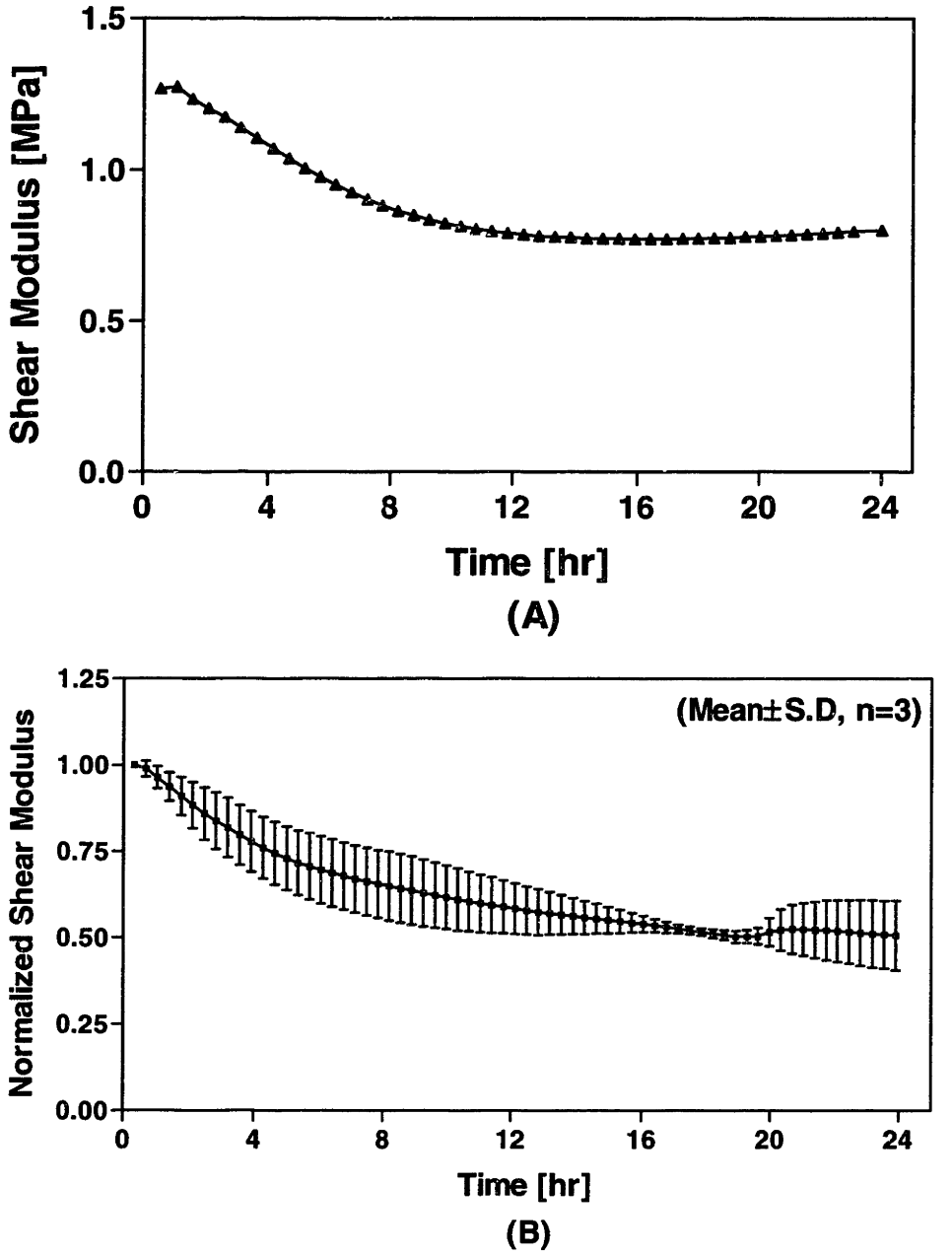

Figure 4-6: Shear modulus decreased initially and after that reached a plateau. Torque was measured every 30 minutes, and each triangle represents calculated shear modulus of 6 samples (A).

4.4 Discussion

Researchers demonstrated the roles of cytoskeleton and cell shape/volume changes in modulating collagen phenotype [2, 1, 10], sulfate incorporation by chondrocytes [35], and intracellular cAMP level [49, 50]. To investigate whether pure mechanical deformation can increase the biosynthetic response of chondrocytes, tissue shear strain which involves no or little relative fluid motion was applied to cartilage explants. Cyclic shear strain of 0.1 Hz and 1% amplitude on articular cartilage plugs increased the incorporation rate of ^{3}H-proline and ^{35}S-sulfate compared to static control and free swelling control. More than 98% of sulfate is incorporated into the GAG molecules of proteoglycan, and for young calf cartilage, approximately 80% of proline is incorporated into collagen molecules [41]. So proline and sulfate incorporation in this experiment can be a good indicator of biosynthetic response of chondrocytes. Even if cartilage samples are under simple shear strain, considering the amplitude of sinusoid was 1%, the relative fluid motion will be limited to the outer edge and the magnitude of fluid velocity will be small. The effect of dynamic axial compression of 0.1 Hz and less than 10% amplitude on the biosynthetic response of chondrocytes was bigger in outer ring region than 2 mm core region and this was consistent with the radial profiles of fluid velocity and streaming potential, but opposite to the profile of hydrostatic pressure [22]. Also the effect of cell deformation can explain the bigger increase of biosynthetic response in outer ring region, since changes in cell volume may occur preferentially in the outer radial periphery. Figure 4-7 (solved by Levenston, M L [28]) shows the finite element solution of fluid velocity and pressure distribution of cartilage when it is deformed by 1% shear strain at 0.1 Hz. It shows that fluid motion is restricted to the trailing and leading edge, and nearly no fluid is induced in the center region.

The comparison of incorporation in core and ring region under dynamic shear strain and control (Figure 4-5) together with the fluid velocity and pressure distribution of finite element solution can imply: 1) the local stimulation by relative fluid motion which can be induced near radial periphery was negligible, 2) the increased

biosynthetic effect by shear strain was due to cellular deformation.

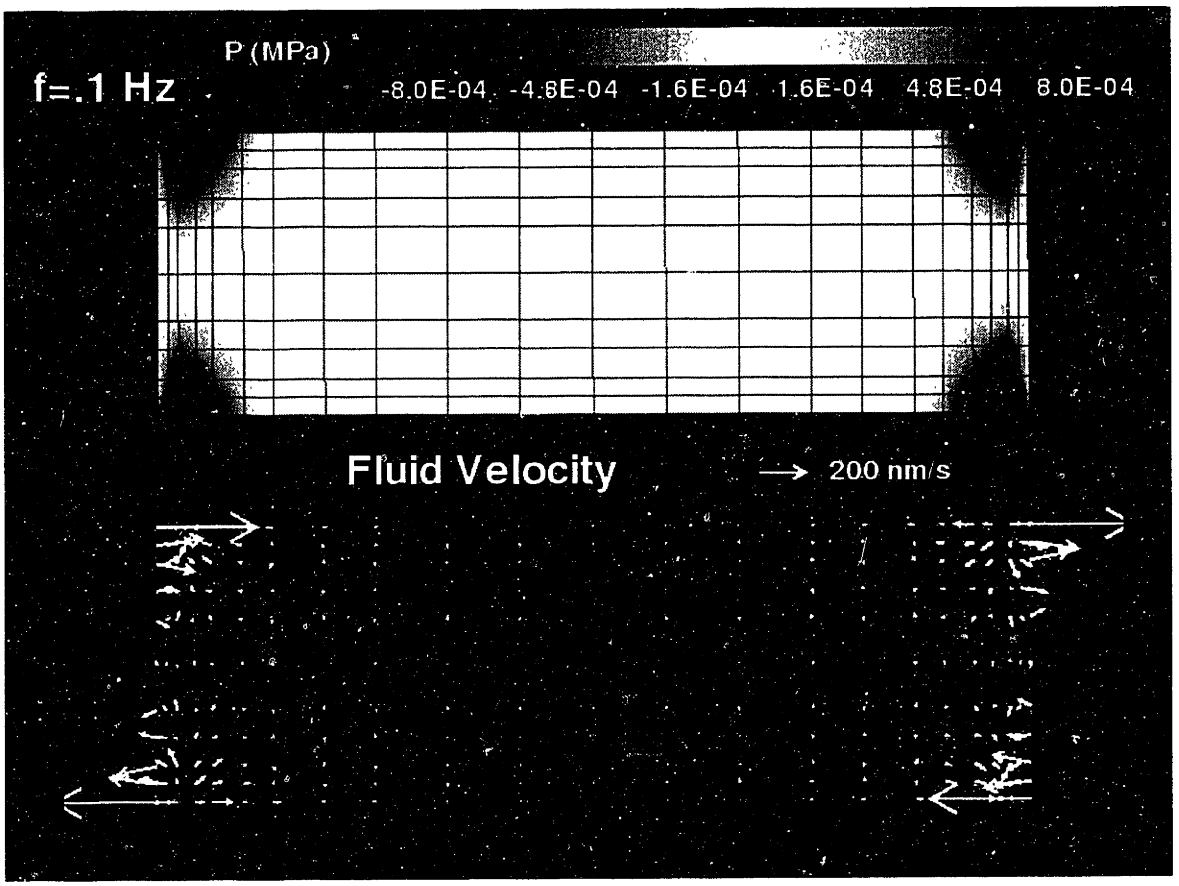

Figure 4-7: Finite element solutions of fluid velocity and pressure distribution within cartilage matrix modeled as a poroelastic material under 0.1 Hz and 1% shear strain application. Majority of fluid flow is localized in the trailing and leading edges of cartilage.

During 24 hr application of shear strain, the measured shear modulus was decreased initially and reached a plateau (Figure 4-6). Mechanical measurement of shear properties of articular cartilage under shear strain greater than ~3% showed similar torque waveform, which indicates the slipping between cartilage and platens, so the decrease in shear modulus in this case can be explained similarly. After 24 hr loading the upper chamber was moved up 500μm and after several minutes back to original position, and shear modulus was measured again. Every measurement showed the decrease in shear modulus was irreversible. Simon [44] reported that a rapid, irreversible

decrease of $\sim$ 35% of initial modulus was observed during application of 90,000 cycles of $\pm$5, $\pm$10, and $\pm$15% of sinusoidal shear strain, and after small magnitude of decay in shear modulus compared to the initial decay, the shear modulus reached a relatively constant point. Compared to their experiment, the cartilage tissue in our experiment was under $\sim$9,000 cycles of 1% sinusoidal shear strain, so the softening of shear modulus may not be explained by the hypothesis that a realignment of the collagen fibrillar matrix or a subtle change in the proteoglycan-collagen interaction. However, considering the shear strain Simon [44] used was at 100 Hz during 3 hr, and in the present experiments, the shear strain was at 0.1 Hz during 24 hr, the mechanism which may be related with the decrease in shear modulus is not necessarily proportional to the applied cycles of shear, but may also be related with the frequency and duration of shear strain. Mechanical properties of collagen and aggregan should be investigated before such a mechanism can be confirmed.

Chapter 5

Summary and Future Work

5.1 Summary

We have previously reported using an incubator-housed compression system to study the effects of axial dynamic compression on the response of cartilage to IGF-1 [6], and on the effects of dynamic compression on biosynthesis by chondrocytes seeded into alginate gel disks [40]. The new biaxial loading apparatus described here has performed well in an incubator environment, accurately applying desired compressive or shear strains to cartilage explants. We have been able to perform both material property testing in addition to metabolic studies of tissue in shear and compression in a sterile incubator environment. Shear modulus tests have been performed in both torsional (pure shear mode) and simple shear modes on similar cartilage disks to validate our measurement methodology. The control software allows axial or rotational ramps and sinusoids of various amplitudes to be intermixed and repeated according to any desired protocol.

The biomechanical properties of articular cartilage explants tested in simple shear agreed well with reported viscoelastic shear properties of articular cartilage [46, 55], demonstrating an increased dynamic stiffness with increased frequency and compressive offset strain. The softening effect we observed with increasing strain amplitude is in agreement with previous reports of nonlinear viscoelastic behavior in cartilage [43] and meniscus [54]. Comparable shear moduli and softening effects were observed

in separate low strain torsional (pure shear mode) tests of 8.4 mm diameter cartilage disks using the same apparatus 3-2 and in verification experiments in which sandpaper was glued to the loading platens. At shear strains greater than 3.0% in mechanical tests, we noted distorted torque waveforms indicative of slipping.

In the metabolic studies, 0.1 Hz dynamic shear deformation produced significant increases in synthesis of proteoglycans and proteins. Unlike pure shear deformation, small amplitude simple shear deformation may induce low levels of fluid flow localized near the leading and trailing edges of the explants (due to bending-induced pressure gradients). As fluid flow has been associated with metabolic stimulation in dynamic unconfined compression studies [24] and fluid induced shear of chondrocytes in monolayer [45], this raises the possibility of local stimulation by fluid flow near the outer edge of the disks subjected to simple shear. In our experiments, however, fluid velocities resulting from macroscopic matrix shear deformation are substantially lower than that in axially compressed disks [24], and many orders of magnitude lower than that in monolayer studies [45]. Finite element model simulations of cartilage mechanical response [28] indicate that fluid flow and fluid pressure gradients in response to dynamic simple shear are confined to the edges, but with amplitudes that are less than 1% of those induced by axial compression (at equal axial compression and shear strain amplitudes). The fact that both the core region (with no fluid flow) and outer annular region of the explants showed comparable metabolic stimulation in response to matrix shear (in contrast to significant ring vs. core differences found by Kim et al [24] for axial compression) suggests that matrix shear deformation, not fluid flow, is responsible for the metabolic stimulation seen in the data of Figure 4-4, 4-5.

5.2 Future Work

In the present study, cartilage disks were under sinusoidal amplitude of 1% at a frequency of 0.1 Hz. Biosynthetic response of chondrocytes under dynamic axial compression increased at frequencies > 0.001 Hz, and at 0.1 Hz frequency the increased biosynthetic response was localized in the outer ring region. So it will be interest-

ing to study cartilage metabolism under different frequencies of shear strain. Also autoradiography can be used to assess matrix synthesis and deposition around chondrocytes, and this method will be useful to check whether the stimulatory effect of shear deformation is localized or not.

Axial compression is known to affect mRNA levels for aggrecan and collagen type II [39]. Under axial compression, chondrocyte metabolism is affected by fluid flow, streaming potential, hydrostatic pressure, and cell/matrix deformation, so it will be important to examine differencies in gene expression under dynamic shear deformation. To investigate the possible mechanism of shear deformation on the biosynthetic response of chondrocytes, microfilament disrupting agent, dihydrocytochalasin B (DHCB), can be used to study the role of cytoskeleton in increased response of chondrocytes under shear deformation.

In the present study, the mechanical behavior of cartilage was measured under different shear strains and frequencies of sinusoid, compressive offset, and ionic strengths. Strain softening and the shear modulus change in different ionic strengths were not investigated enough to explain those experimental observations. More extensive study of collage and proteoglycan characteristics and their interactions will be necessary for better explanations.

Appendix A

Drawing of Machine Design

A.1 Machine Components

Figure A-1 shows a schematic drawing of the machine. Abbreviations for each components are written on corresponding parts. Table A.1 shows components lists and referring pages.

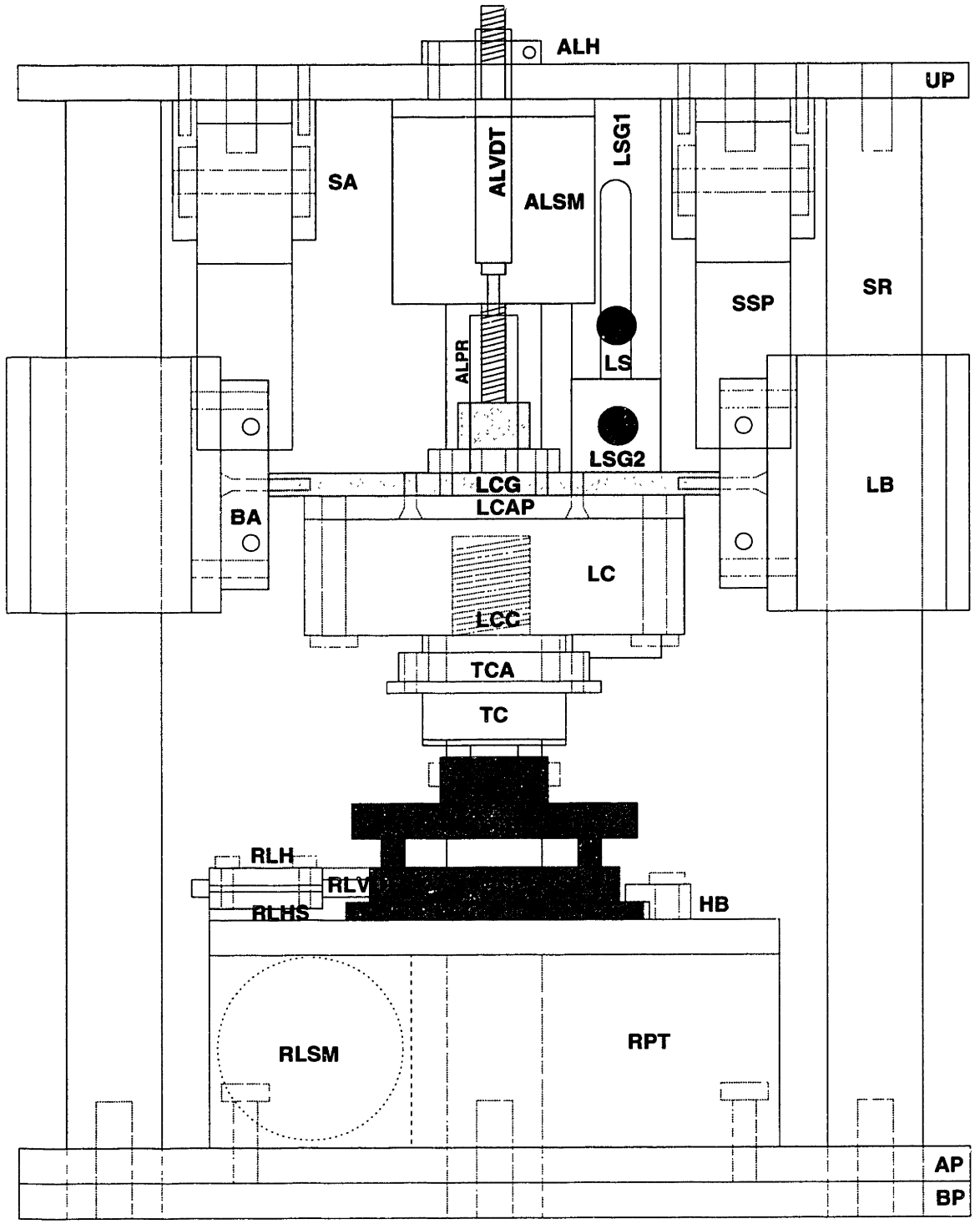

Figure A-1: Schematic drawing of a shear loading apparatus.

Table A.1: Components of Shear Application Machine

Components	Acronym	Page
Axial LVDT Holder	ALH	70
Axial LVDT Position Rod	ALPR	70
Axial Linear Stepper Motor	ALSM	19
Axial LVDT	ALVDT	19
Adjusting Plate	AP	72
Bearing Adapter	BA	69
Bottom Chamber	BCB	22
Bottom Plate	BP	73
Chamber Holding Block	CHB	75
Linear Bearing	LB	
Load Cell	LC	21
Load Cell Adapter Plate	LCAP	69
Load Cell Connector	LCC	69
Load Carriage Adapter Plate	LCAP	69
Limit Sensor	LS	
Limit Sensor Guide I	LSG1	70
Limit Sensor Guide II	LSG2	70
Rotational LVDT Holder	RLH	75
Rotational LVDT Holder Support	RLHS	75
Rotational LVDT Position Block	RLPB	70
Rotational Linear Steppter Motor	RLSM	19
Rotational LVDT	RLVDT	19
Rotary Positioning Table	RPT	19
Spring Holder	SA	70
Supproting Rod	SR	74
Sheet Spring	SSP	
Top Plate	TP	71
Torque Cell	TC	21
Torque Cell Adapter	TCA	
Top Chamber	TCB	22

A.2 Drawing of Machine Components

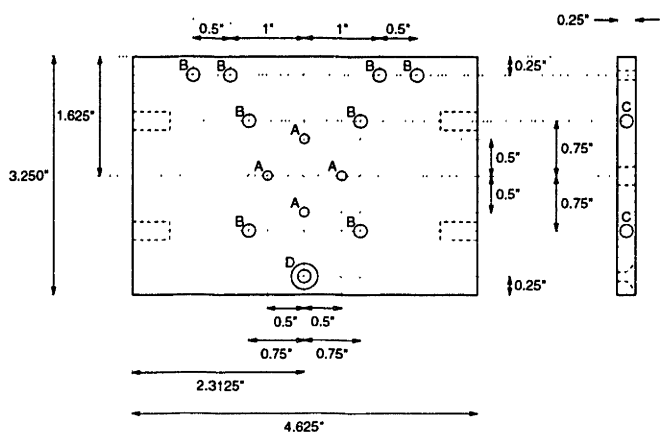

Load Carriage
Material: 4.625" x 3.250" x 0.25" thick Stainless Steel

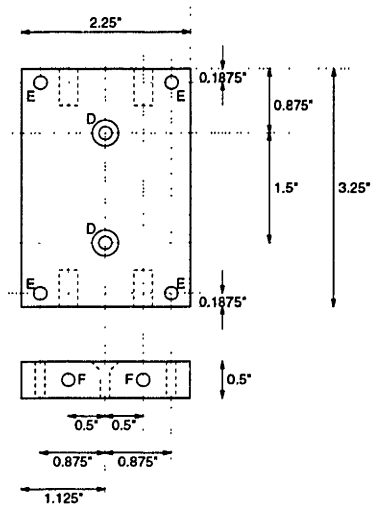

Bearing Adapter
Material: 3.25" x 2.25" x 0.5" Aluminum
2 pieces

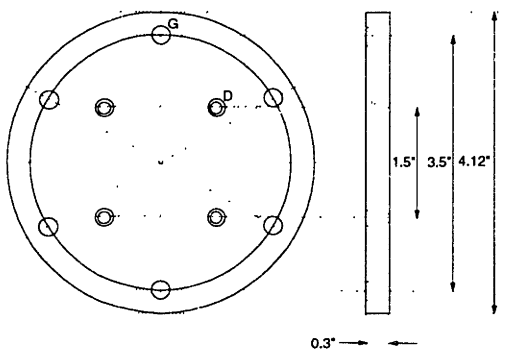

Load Cell Adapter Plate
Material: Aluminum

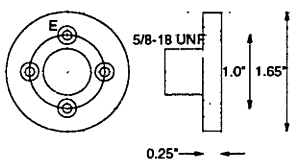

Load Cell Connector
Material: Aluminum

HOLE INDEX:
A: #36 drill (0.106") and tap for 6-32 thread
B: #29 drill (0.136") and tap for 8-32 thread
C: #29 drill (0.136") and tap for 8-32 thread x 0.5" deep
D: #19 drill (0.166") and countersink for 8-32 flat head screw
E: #21 drill (0.159") and tap for 10-32 thread
F: #21 drill (0.159") and tap for 10-32 thread x 0.5" deep
G: #7 drill (0.25") and tap for 1/4 -20 thread

Figure A-2: Adapters: Bearing Adapter (BA), Load Carriage (LCG), Load Cell Adapter Plate (LCAP), Load Cell Conector (LCC)

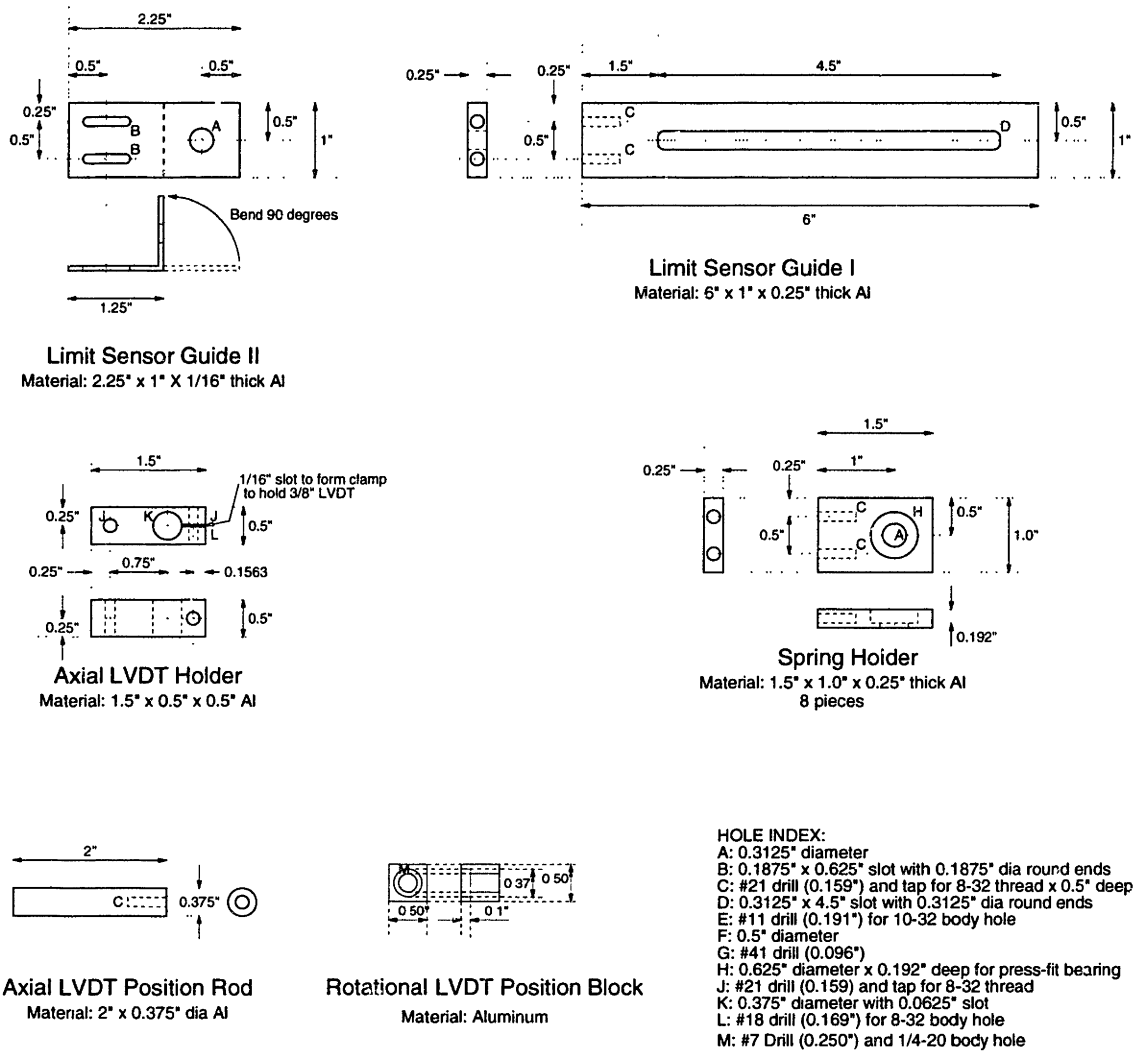

Figure A-3: Miscellaneous Parts: Limit Sensor Guide (LSG) I II, Axial LVDT Holder (ALH), Spring Holder (SH), Axial LVDT Position Rod (ALPR), Rotational LVDT Position Block (RLPB)

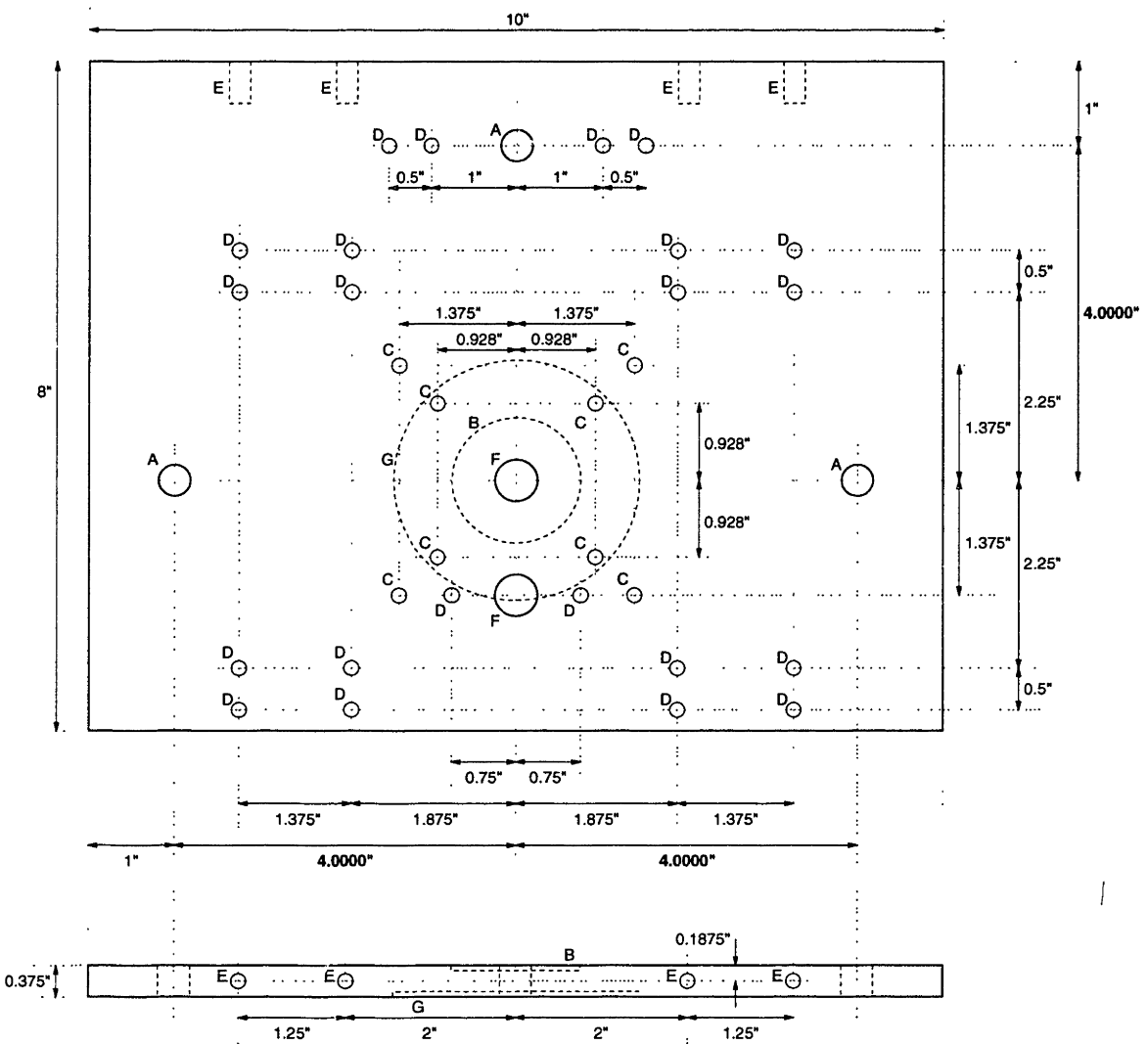

HOLE INDEX:
A: Size V drill (0.377" diameter)
B: 1.504" + 0.002" - 0.000" dia x 0.0625" deep (NOTE: minimum size)
C: #21 drill (0.159") and tap for 10-32 thread
D: #18 drill (0.169") for 8-32 body hole
E: #21 drill (0.159") and tap for 10-32 thread x 0.5" deep centered on edge of plate
F: 0.5" diameter
G: 2.878" + 0.002" - 0.000" dia x 0.0625" deep (on opposite side from B)

Top Plate

Material: 10" x 8" x 0.375" Stainless Steel

Figure A-4: Top Plate

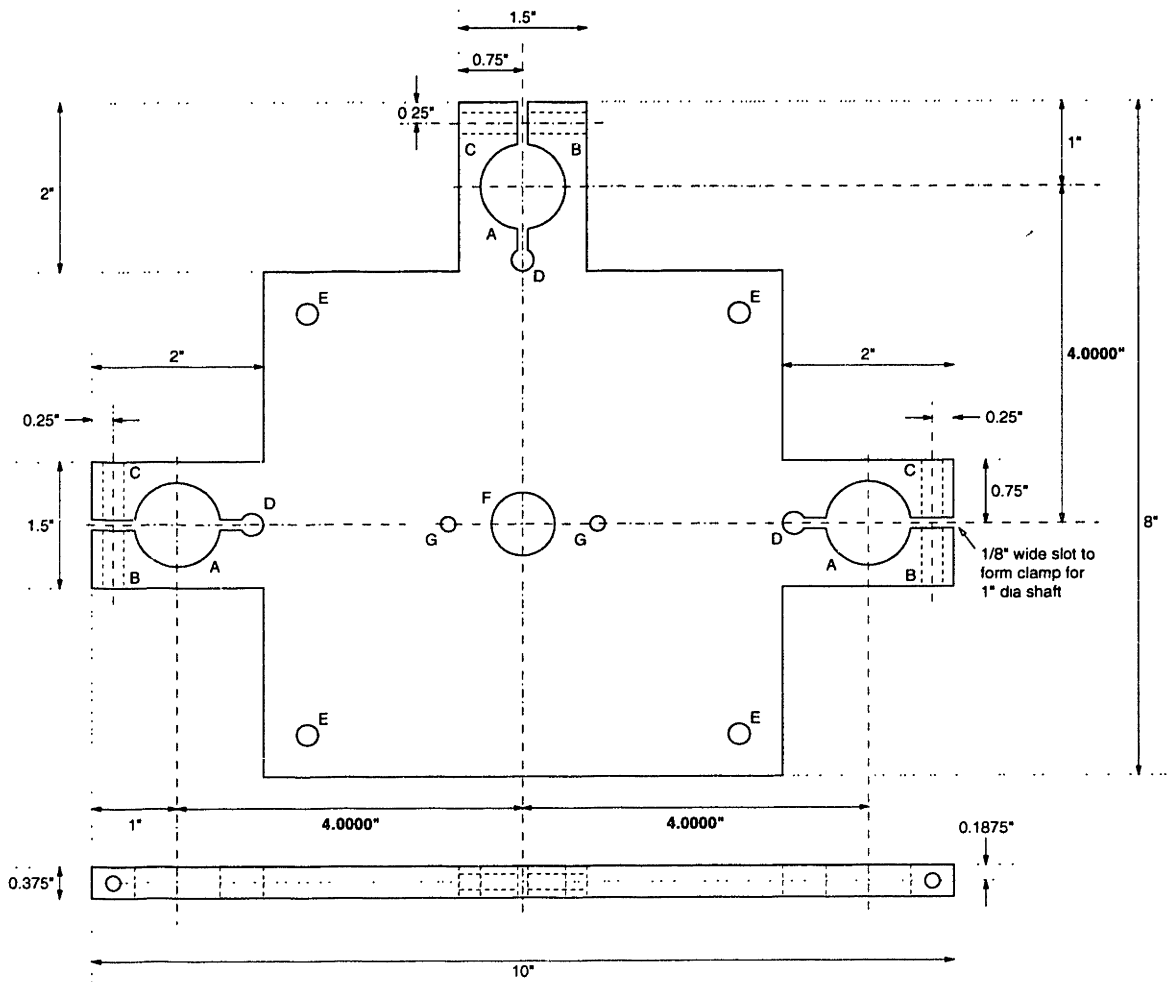

HOLE INDEX:
A: 1.000" diameter with 0.125" slot cut as shown
B: #9 drill (0.196") for 10-32 body hole
C: Drill and tap for 10-32 thread
D: 0.25" diameter for stress relief, continue 0.125 slot from A to D as shown
E: Drill and tap for 1/4-20 thread
F: 0.75" diameter
G: Drill and tap for 8-32 thread

Adjusting Plate

Material: 10" x 8" x 0.375" Stainless Steel

Figure A-5: Adjusting Plate

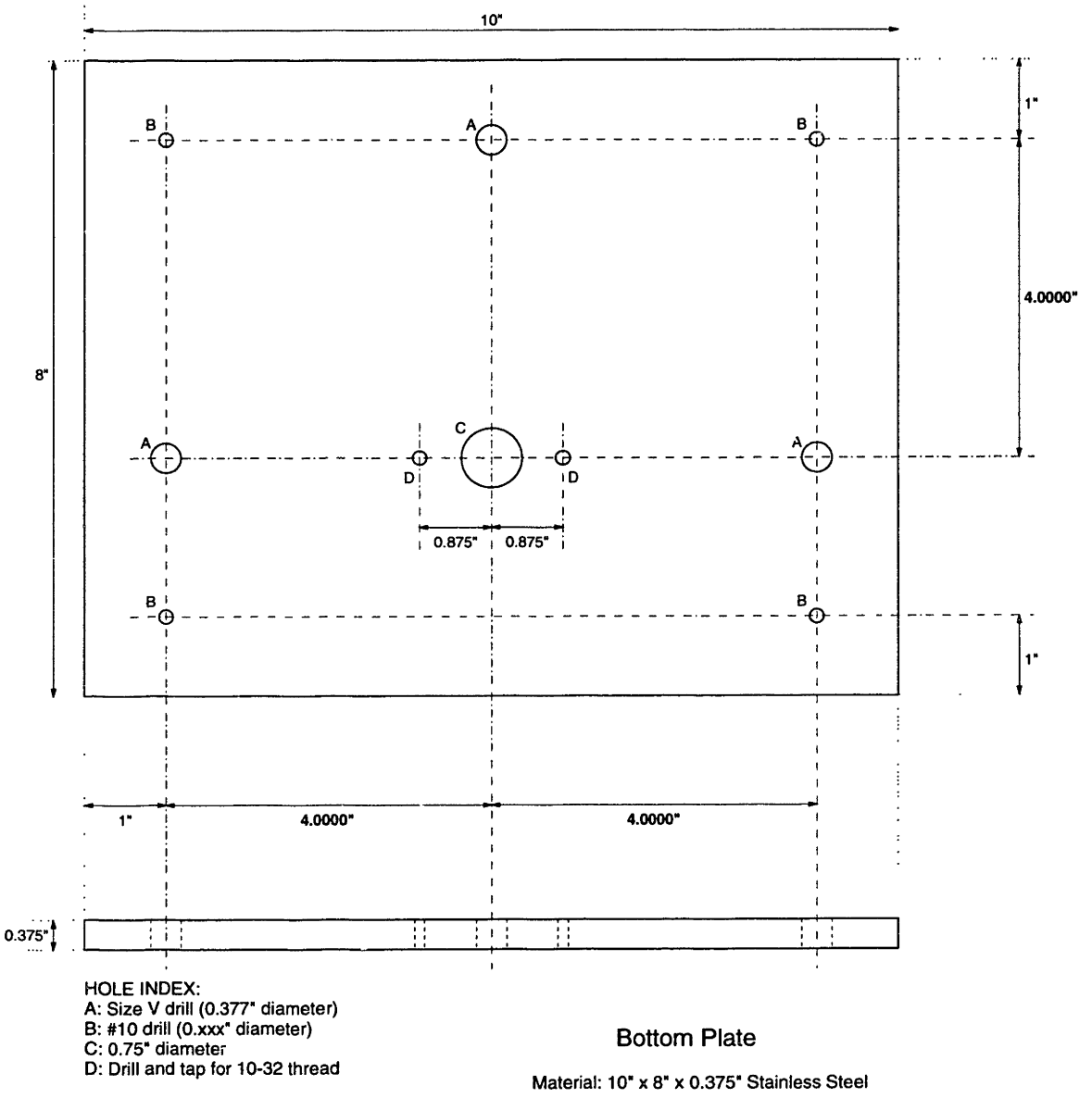

Figure A-6: Bottom Plate

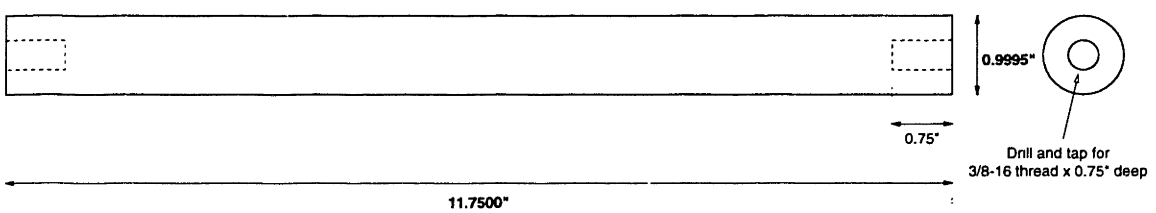

Supporting Rod

Material: 11.75" x 0.9995" diameter Stainless Steel Precision Shaft, hardened and ground

3 pieces cut to exact same length

Figure A-7: Supporting Rod

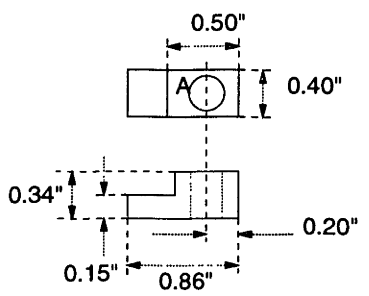

Chamber Holding Block
Material : Aluminum

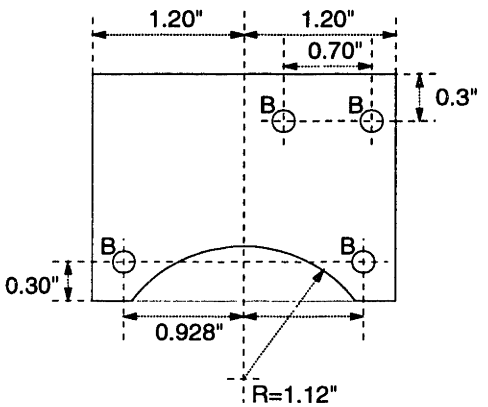

Rotational LVDT Holder Support
Material : Stainless Steel, 0.3" Thickness

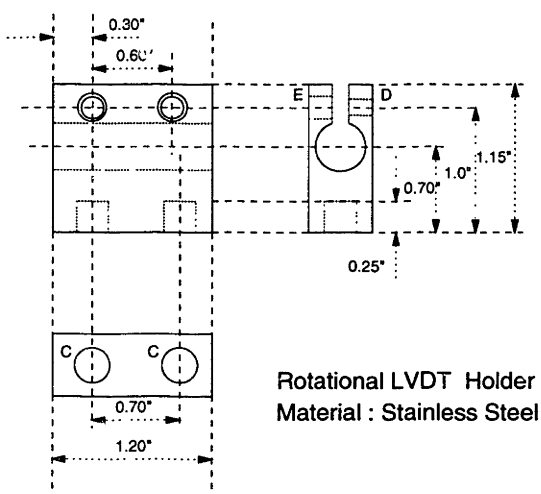

Rotational LVDT Holder
Material : Stainless Steel

HOLE INDEX:
A: F drill (0.2570") for 1/4-20 body hole
B: #9 drill (0.1960) for 10-32 body hole
C: #21 drill (0.19") and tap for 10-32 thread X 0.25" deep
D: #29 drill (0.1640") and tap for 8-32 thread
E: #18 drill (0.1695") for 8-32 body hole

Figure A-8: Holders: Chamber Holding Block (CHB), Rotational LVDT Holding Support (RLHS), Rotational LVDT Holder (RLH)

Bibliography

[1] P D Benya, P D Brown, and S R Padilla. Microfilament modification by dihydrocytochalasin B causes retinoic acid-modulated chondrocytes to reexpress the differentiated collagen phenotype without a change in shape. *Journal of Cell Biology*, 106:161–170, 1988.

[2] P D Benya and J D Shaffer. Dedifferentiated chondrocytes reexpress the differentiated chondrocyte phenotype when cultured in agarose gels. *Cell*, 30:215–224, 1982.

[3] M A Biot. General theory of three-dimensional consolidation. *Journal of Applied Physics*, 12:155–164, 1941.

[4] M A Biot. Theory of elasticity and consolidation for a porous anisotropic solid. *Journal of Applied Physics*, 26:182–185, 1955.

[5] A J Bodine, N Brown, W C Hayes, and S A Jiminez. The effect of sodium chloride on the shear modulus of articular cartilage. In *Transactions of the Orthopaedic Research Society*, page 37, Atlanta, GA, 1980.

[6] L J Bonassar, A J Grodzinsky, S G Davila, and S B Trippel. The effects of dynamic compression on the response of cartilage to IGF-1. In *Transactions of the Orthopaedic Research Society*, volume 23, page 579, New Orleans, LA, 1998.

[7] F Bonnet, D G Dunham, and T E Hardingham. Structure and interactions of cartilage proteoglycan binding region and link protein. *Biochemical Journal*, 228:78–85, 1985.

[8] R M Bowen. Incompressible porous media models by use of the theory of mixtures. *International Journal of Engineering Science*, 18:1129–48, 1980.

[9] N D Broom. Abnormal softening in articular cartilage: its relationship to the collagen framework. *Arthritis and Rheumatism*, 25:1209–1216, 1982.

[10] P D Brown and P D Benya. Alterations in chondrocyte cytoskeletal architecture during phenotypic modulation by retinoic acid and dihydrocytochalasin b-induced reexpression. *Journal of Cell Biology*, 106:171–179, 1988.

[11] S R Eisenberg and A J Grodzinsky. The kinetics of chemically induced nonequilibrium swelling of articular cartilage and corneal stroma. *Journal of Biomechanical Engineering*, 109:79–89, 1987.

[12] R W Farndale, D J Buttle, and A J Barrett. Improved quantitation and discrimination of sulphated glycosaminoglycans by use of dimethylmethylene blue. *Biochimica et Biophysica Acta*, 883:173–177, 1986.

[13] J D Ferry. *Viscoelastic Properties of Polymers*. John Wiley Sons, INC, 1970.

[14] E H Frank and A J Grodzinsky. Cartilage electromechanics-II. A continuum model of cartilage electrokinetics and correlation with experiments. *Journal of Biomechanics*, 20:629–639, 1987.

[15] E H Frank, A J Grodzinsky, S L Phillips, and P E Grimshaw. Physicochemical and bioelectrical determinants of cartilage material properties. In V C Mow, A Ratcliffe, and S L Y Woo, editors, *Biomechanics of Diarthrodial Joints*, pages 261–282. Springer-Verlag, New York, NY, 1990.

[16] N J Giori, G S Beaupré, and D R Carter. Cellular shape and pressure may mediate mechanical control of tissue composition in tendons. *Journal of Orthopaedic Research*, 11:581–91, 1993.

[17] A J Grodzinsky. Electromechanical and physicochemical properties of connective tissue. *CRC Critical Reviews in Bioengineering*, 9:133–199, 1983.

[18] A J Grodzinsky, Y J Kim, M D Buschmann, T M Quinn, A M Garcia, and E B Huziker. Response of the chondrocyte to mechanical stimuli. In K D Brandt, M Doherty, and L S Lohmander, editors, *Osteoarthritis*, pages 123–136. Oxford University Press, 1998.

[19] A C Hall, J P G Urban, and K A Gehl. The effects of hydrostatic pressure on matrix synthesis in articular cartilage. *Journal of Orthopaedic Research*, 9:1–10, 1991.

[20] W C Hayes and A J Bodine. Flow-independent viscoelastic properties of articular cartilage matrix. *Journal of Biomechanics*, 11:407–419, 1978.

[21] W C Hayes and L F Mockros. Viscoelastic properties of human articular cartilage. *Journal of Applied Physiology*, 31:562–568, 1971.

[22] Y-J Kim, L J Bonassar, and A J Grodzinsky. The role of cartilage streaming potential, fluid flow and pressure in the stimulation of chondrocyte biosynthesis during dynamic compression. *Journal of Biomechanics*, 28:1055–1066, 1995.

[23] Y-J Kim, R L Y Sah, J Y H Doong, and A J Grodzinsky. Fluorometric assay of DNA in cartilage explants using Hoechst 33258. *Analytical Biochemistry*, 174:168–176, 1988.

[24] Y-J Kim, R L-Y Sah, A J Grodzinsky, A H K Plaas, and J D Sandy. Mechanical regulation of cartilage biosynthetic behavior: Physical stimuli. *Archives of Biochemistry and Biophysics*, 311:1–12, 1994.

[25] M K Kwan, W M Lai, and V C Mow. A finite deformation theory for cartilage and other soft hydrated connective tissues—I. equilibrium results. *Journal of Biomechanics*, 23:145–155, 1990.

[26] M K Kwan, J S Wayne, S L-Y Woo, F P Field, J Hoover, and M Meyers. Histological and biomechanical assessment of articular cartilage from stored osteochondral shell allografts. *Journal of Orthopaedic Research*, 7:637–644, 1990.

[27] M E Levenston, E H Frank, and A J Grodzinsky. Variationally derived 3-field lagrange multiplier and augmented lagrangian poroelastic finite elements for soft tissues. In *Advances in Bioengineering: ASME-BED*, volume 33, pages 145–6, Atlanta, 1996.

[28] M E Levenston, E H Frank, and A J Grodzinsky. Variationally derived 3-field finite element formulations for quasistatic poroelastic analysis of hydrated biological tissues. *Computer methods in applied mechanics and engineering*, 156:231–246, 1998.

[29] A Maroudas. Balance between swelling pressure and collagen tension in normal and degenerate cartilage. *Nature*, 260:808–809, 1976.

[30] A Maroudas. Physicochemical properties of articular cartilage. In M A R Freeman, editor, *Adult Articular Cartilage, 2nd ed.*, pages 215–290. Pitman, Tunbridge Wells, England, 1979.

[31] V C Mow, S C Kuei, W M Lai, and C G Armstrong. Biphasic creep and stress relaxation of articular cartilage in compression: Theory and experiments. *Journal of Biomechanical Engineering*, 102:73–84, 1980.

[32] V C Mow, A F Mak, and W M Lai. Viscoelastic properties of proteoglycan subunits and aggregates in varying solution concentrations. *Journal of Biomechanics*, 17(5):325–338, 1984.

[33] Helen Muir. The chondrocyte, architect of cartilage. *BioEssays*, 17(12):1039–1048, 1995.

[34] I H M Muir. The chemistry of the ground substance of joint cartilage. In L Sokoloff, editor, *The Joints and Synovial fluid*, volume II, pages 27–94. Academic Press, New York, 1980.

[35] P Newman and F M Watt. Influence of cytochalasin d-induced changes in cell shape on proteoglycan synthesis by cultured articular chondrocytes. *Experimental Cell Research*, 178:199–210, 1988.

[36] I A Nieduszynski, J K Sheehan, C F Phelps, T E Hardingham, and H Muir. Equilibrium-binding studies of pig laryngeal cartilage proteoglycans with hyaluronate oligosaccharide fractions. *Biochemical Journal*, 185:107–114, 1980.

[37] J J Parkkinen, J Ikonen, M J Lammi, J Laakkonen, and M Tammi. Effects of cyclic hydrostatic pressure on proteoglycan synthesis in cultured articular chondrocytes and cartilage explants. *Archives of Biochemistry and Biophysics*, 300:458–465, 1993.

[38] J R Parsons and J Black. The viscoelastic shear behavior of normal rabbit articular cartilage. *Journal of Biomechanics*, 10:21–29, 1977.

[39] P M Ragan, A M Badger, R A Dodds, M Cook, J R Connor, A J Grodzinsky, and M W Lark. Mechanical compression affects chondrocyte matrix gene expression in cartilage explants. In *Transactions of the Orthopaedic Research Society*, volume 23, page 918, New Orleans, LA, 1998.

[40] P M Ragan, A K Staples, H K Hung, V I Chin, F Binette, and A J Grodzinsky. Mechanical compression influences chondrocyte metabolism in a new alginate disk culture system. In *Transactions of the Orthopaedic Research Society*, volume 12, page 991, New Orleans, LA, 1998.

[41] R L Sah, Y-J Kim, J H Doong, A J Grodzinsky, A H K Plaas, and J D Sandy. Biosynthetic response of cartilage explants to dynamic compression. *Journal of Orthopaedic Research*, 7:619–636, 1989.

[42] R K Schenk, P S Eggli, and E B Hunziker. Articular cartilage morphology. In K E Kuettner, R Schleyerbach, and V C Hascall, editors, *Articular Cartilage Biochemistry*, pages 3–22. Raven Press, New York, 1986.

[43] W H Simon, A Mak, and A Spirt. The effect of shear fatigue on bovine articular cartilage. *Journal of Orthopaedic Research*, 8:86–93, 1990.

[44] William H Simon, Arthur Mak, and Adrienne Spirt. The effect of shear fatigue on bovine articular cartilage. *Journal of Orthopaedic Research*, 8:86–93, 1989.

[45] R L Smith, B S Donlon, M K Gupta, M Mohtai, P Das, D R Carter, J Cooke, G Gibbons, N Hutchinson, and D J Schurman. Effects of fluid-induced shear on articular chondrocytes morphology and metabolism *in vitro*. *Journal of Orthopaedic Research*, 13:824–831, 1995.

[46] A A Spirt, A F Mak, and R P Wassel. Nonlinear viscoelastic properties of articular cartilage in shear. *Journal of Orthopaedic Research*, 7:43–49, 1989.

[47] J P G Urban, A C Hall, and K A Gehl. Regulation of matrix synthesis rates by the ionic and osmotic environment of articular chondrocytes. *Journal of Cellular Physiology*, 154:262–270, 1993.

[48] J P G Urban, A Maroudas, M T Bayliss, and J Dillon. Swelling pressures of proteoglycans at the concentrations found in cartilaginous tissues. *Biorheology*, 16:447–464, 1979.

[49] P A Watson. Accumulation of camp and calcium in s49 mouse lymphoma cells following hyposmotic swelling. *Journal of Biological Chemistry*, 264:14735–14740, 1989.

[50] P A Watson. Direct stimulation of adenylate cyclase by mechanical forces in s49 mouse lymphoma cells during hyposmotic swelling. *Journal of Biological Chemistry*, 265:6569–6575, 1990.

[51] S L Woo, M A Gomez, and W H Akeson. The time and history-dependent viscoelastic properties of the cannine medial collateral ligament. *Journal of Biomechanical Engineering*, 103:293–298, 1981.

[52] S L-Y Woo, B R Simon, S C Kuei, and W H Akeson. Quasi-linear viscoelastic properties of normal articular cartilage. *Journal of Biomechanical Engineering*, 102:85–90, 1980.

[53] C E Yellowley, C R Jacobs, Z Li, Z Zhou, and H J Donahue. Effects of fluid flow on intracellular calcium in bovine articular chondrocytes. *American Journal of Pathology*, 273:C30–C36, 1997.

[54] W Zhu, K Y Chern, and V C Mow. Anisotropic viscoelastic shear properties of bovine meniscus. *Clinical Orthopaedics and Related Research*, 306:34–45, 1994.

[55] W Zhu, V C Mow, T J Koob, and D R Eyre. Viscoelastic shear properties of articular cartilage and the effects of glycosidase treatments. *Journal of Orthopaedic Research*, 11:771–781, 1993.

THESIS PROCESSING SLIP

FIXED FIELD: ill. _____ name _____

index _____ biblio _____

▶ COPIES: (Archives) Aero Dewey (Eng) Hum
Lindgren Music Rotch Science

TITLE VARIES: ▶ ☐ _____

NAME VARIES: ▶ ☐ _____

IMPRINT: (COPYRIGHT) _____

▶ COLLATION: 82 l

▶ ADD: DEGREE: _____ ▶ DEPT.: _____

SUPERVISORS: _____

NOTES:

cat'r: date:

page: F 37

▶ DEPT: M.E.

▶ YEAR: 1999 ▶ DEGREE: S.M.

▶ NAME: JIN, Moonsoo